CHAPTER 6

Time-Resolved Laser-Induced Incandescence

Alfred Leipertz and **Roland Sommer**

Contents

Abstract

Online characterization of nanoscaled particles is an important issue in basic research, e.g., combustion soot formation and oxidation, and in several different technical applications, e.g., in nanoparticle production reactors or in automotive raw exhaust. For the determination of mass concentration and primary particle size, a possible in situ measurement technique is time-resolved laser-induced incandescence (TIRE-LII). The basic principle of this technique is the heating-up of the nanoscaled particles by a high-energetic laser pulse and the subsequent detection and analysis of the spectrally and temporally resolved enhanced thermal

Department of Engineering Thermodynamics and Erlangen Graduate School in Advanced Optical Technologies, University of Erlangen-Nuremberg, Am Weichselgarten 8, 91058 Erlangen, Germany

Advances in Chemical Engineering, Volume 37
ISSN: 0065-2377, DOI 10.1016/S0065-2377(09)03706-5

radiation. At later times after the laser pulse, heat conduction to the ambient gas is the dominant heat loss mechanism and so particles with different specific surface area cool down differently. From the temporal signal decay, the size distribution of the primary particles can be derived. Furthermore, the signal maximum is proportional to the mass concentration. Here, besides an introduction to the basic principle of this technique, an overview is given on current technical applications using this measurement technique and on its use in basic combustion research, for nanoparticle characterization, with emphasis on carbonaceous particles. Measurements have been performed at different nanoparticle production reactors on the one hand side and directly in the diesel engine raw exhaust and in ambient air on the other hand. Thereby, the results were compared with established measurement methods such as transmission electron microscopy (TEM), conventional adsorption analysis and gravimetrical techniques. Furthermore, a new approach is shown applying this technique also in liquids for suspended particles.

1. INTRODUCTION

The industrial production of nanoscaled particles has become very important in recent years due to the increased number of application areas of these materials. Exemplarily, carbon blacks are important nanoparticles, which are included as crucial additives in tires, paints and varnishes. One particle property that determines together with other attributes the quality of these products is the primary particle size. To measure and control this quantity during the production process, an appropriate size characterization method is required. For this, online and in situ process monitoring is necessary. Other areas in which the characterization of carbonaceous particles plays an important role are soot measurements in engines, mainly diesel raw exhaust and in ambient air. Unfortunately, current measurement techniques such as transmission electron microscopy (TEM), chemical analysis, dynamic light scattering (DLS), impactors or scanning mobility particle sizers (SMPS) do not allow fast, non-intrusive or selective determination. This is however possible using time-resolved laser-induced incandescence (TIRE-LII).

Laser-induced incandescence (LII) has been proven to be a powerful measurement tool for soot characterization in different flames for many years. First theoretical considerations for soot characterization by laser heating were proposed by Melton (1984), followed by first experimental investigations by Dasch (1984). Basic approaches for the determination of the soot concentration have been carried out by Tait and Greenhalgh (1993); Vander Wal and Wieland (1994) and Vander Wal and Choi (1995).

First quantitative investigations in flames were conducted in the following years by different groups (Shaddix and Smyth, 1996; Mewes and Seitzman, 1997). The determination of the primary particle size was first experimentally conducted by Will et al. (1995, 1998) introducing the TIRE-LII technique and nearly at the same time by Roth and Filippov (1996). In recent years it has been further developed for particle characterization in technically important systems (see, e.g., in Leipertz and Dankers, 2003). Direct accessible parameters are the volume concentration and the primary particle diameter. Meanwhile, it has been extended to evaluate even the size distribution of particles (Lehre et al., 2003; Dankers and Leipertz, 2004). In combination with light scattering measurements, the volume equivalent aggregate particle size and the number of the primary particles per aggregate can also be determined (Will et al., 1996). The potential and features of this technique are presented exemplarily by a few selected measurements, briefly for flame investigations and more extended for the online primary particle size characterization within a carbon black production reactor (Dankers et al., 2003) or the soot analysis in engine exhaust (Schraml et al., 2004). In particular, for engine applications, the method has been implemented to a robust sensor, which allows a reliable soot measurement even for modern low emission vehicles. This sensor has a high temporal resolution of up to 20 Hz and a very low detection limit of just a few $\mu g/m^3$, which qualifies the system also for emission measurement and environmental health control. Moreover, the potential of this measurement technique for particle sizing in suspensions is described. Additional details on the application of this technique can be found in published overview articles (Leipertz et al., 2002; Santoro and Shaddix, 2002; Leipertz and Dankers, 2003). The state of the art in modeling the LII process is described in some detail by Schulz et al., (2006), Michelsen et al. (2007), Michelsen et al. (2008) and in the compilation of several LII-related papers published in a special feature issue in *Applied Physics B*, Vol. 83, 333–485 (2006).

2. MEASUREMENT PRINCIPLE

2.1 Energy balance and LII signal

The basic principle of LII is the rapid heating of nanoparticles often up to their sublimation temperature within a few nanoseconds by means of a short intense laser pulse and the subsequent detection and evaluation of the enhanced thermal radiation. First, the particles are heated up by absorbing the laser radiation, which results in an increased internal energy. Considering carbonaceous particles, their maximum particle

temperatures reached are about 4000–4500 K for a short time period of several nanoseconds. The subsequent heat loss is dominated by different mechanisms, mainly sublimation and heat conduction. The contribution of the thermal radiation to the energy loss is small for all times. By setting up the energy balance for one single particle, the resulting differential equation yields

$$C_{abs}E_i - \Lambda\,(T - T_0)\,\pi d_p^{\,2} + \frac{\Delta H_S}{M}\frac{\mathrm{d}m}{\mathrm{dt}} - \pi d_p^{\,2}\int \varepsilon(d_p,\,\lambda)\,M_\lambda^{\,b}(T,\,\lambda)\,\mathrm{d}\lambda - \frac{\pi d_p^{\,3}}{6}\,\rho c_P\frac{\mathrm{d}T}{\mathrm{dt}} = 0 \tag{1}$$

The temporally resolved particle temperature can be calculated by solving the differential equation including the laser absorption in the Rayleigh-Regime (absorption efficiency C_{abs}, laser energy E_i), heat conduction (Knudsen number dependent heat transfer coefficient Λ, particle temperature T, temperature T_0 of the surrounding gas), sublimation (sublimation enthalpy ΔH_V, molar mass M) and radiation (emission coefficient ε, spectral energy density M_λ^b, wavelength λ), as well as the change of the internal energy (mass density ρ, specific heat c_P). Thereby, Equation 1 includes the assumption of spherical primary particles (diameter d_p), which have only point contact to other particles inside the aggregates. Applying Planck's radiation law, the detectable signal can be determined (Santoro and Shaddix, 2002).

Accurate modeling is only possible by the consideration of wavelength-dependent optical and temperature-dependent thermodynamic parameters and the correct application of the thermal accommodation coefficient which is dependent on the ambient particle conditions and is described in detail elsewhere (Schulz et al., 2006; Daun et al., 2007). Moreover, Michelsen (2003) suggested the inclusion of a nonthermal photodesorption mechanism for heat and mass loss, the sublimation of multiple cluster species from the surface, and the influence of annealing on absorption, emission, and sublimation. A more general form of the energy equation including in more detail mass transfer processes has been derived recently by Hiers (2008). For practical use, Equation (1) turns out to be of sufficient physical detail.

One attribute of this measurement technique is the non-linear behavior of the maximum peak signal with the excitation laser energy. An initial increase in laser fluence leads to a rapid rise in the peak LII signal, whereby it levels off to a so-called "plateau" region at a laser fluence of about 0.2 J/cm^2 for a laser wavelength of 532 nm, from which no significant signal change is evident (Will et al., 1998). This observation is found in previous studies on aerosols and flames (Snelling et al., 2000; Bladh and Bengtsson, 2004). Noteworthy is the plateau width that is strongly dependent on the laser spatial energy distribution. In the

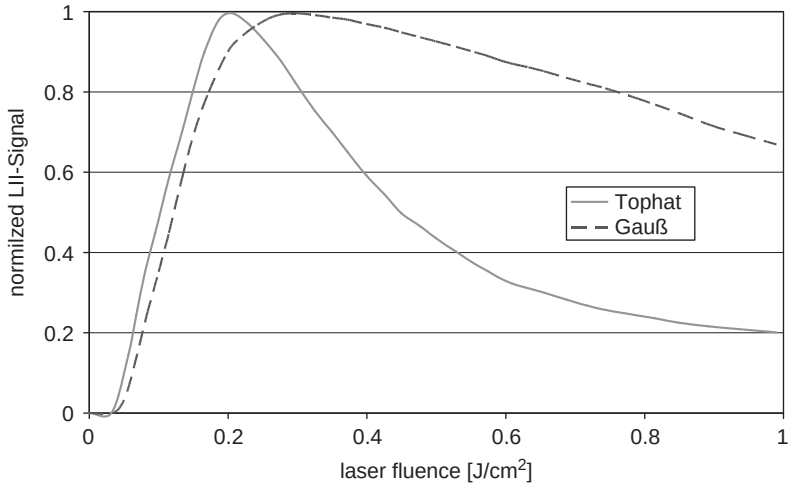

Figure 1 Maximum LII signal dependence on laser fluence.

plateau region, the particles reach their peak temperature, sublimation acting as the limiting factor. At higher laser excitations, the particles shrink due to surface sublimation of carbonaceous matter that, in turn, leads to lower signal intensities. Moreover, due to high laser fluences, morphological changes can also occur possibly modifying the particle properties (Vander Wal et al., 1998; Vander Wal and Choi, 1999). For technical applications, this ''plateau'' region is of advantage as changes in the laser fluence do not affect the signal behavior. In Figure 1 the plateau shape is shown in dependence of the laser spatial profile type.

Under the assumption of sufficiently high laser excitation energies, the heat loss at peak particle temperature is dominated by sublimation. Hence, the maximal signal is proportional to the particle volume

$$S_{\mathrm{LII}} \propto d_p^{\,3+(\lambda/0.154)} \tag{2}$$

by using long detection wavelengths λ (Melton, 1984; Will et al., 1995; Mewes and Seitzman, 1997). If quantitative data for the mass concentration are required, it is necessary to perform an appropriate calibration. This can easily be done by a single line-of-sight extinction measurement or comparison to gravimetric methods.

However, recent studies by Reimann et al. (2008) and Bladh et al. (2008) showed that for atmospheric flame conditions the particle size influences the relationship between ''prompt'' LII signal (maximum LII signal) and the volume concentration to a low degree in the low-fluence regime but has a clear influence in the high-fluence regime. A possible consideration of this is to determine the volume fraction as well as the primary particle size (see Chapter II.B) in parallel.

Even more flexibility of LII can optionally be achieved if it is combined with elastic light scattering, which is discussed in more detail elsewhere (see, e.g., Will et al., 1996). By this also the agglomerate size is accessible. This is, more precisely, an optically equivalent diameter of the agglomerates (radius of gyration), which correlates with the widely determined diffusion diameter of the particles. In this context, it should be pointed out that elastic light scattering in contrast to LII is not selective to the desired fraction of the particles. As also other particle components, e.g., volatiles, contribute to the scattered signal, an appropriate sample conditioning is required for performing combined scattering/LII experiments.

2.2 Determination of primary particle size and its distribution

At later times after the laser pulse heat conduction becomes the dominating heat loss mechanism (Will et al., 1995), and therefore, particles with different specific surface areas cool down differently, which is shown schematically in Figure 2 (Roth and Filippov, 1996; Will et al., 1995, 1998). The local gas temperature adjacent to particles turns out to be the most critical parameter for the accuracy of size determination (Will et al., 1998), which however can be derived from the temperatures of the soot particles themselves (Schraml et al., 2000).

For the determination and evaluation of the LII signal and the decay time, two strategies exist. The complete temporal LII signal decay can be

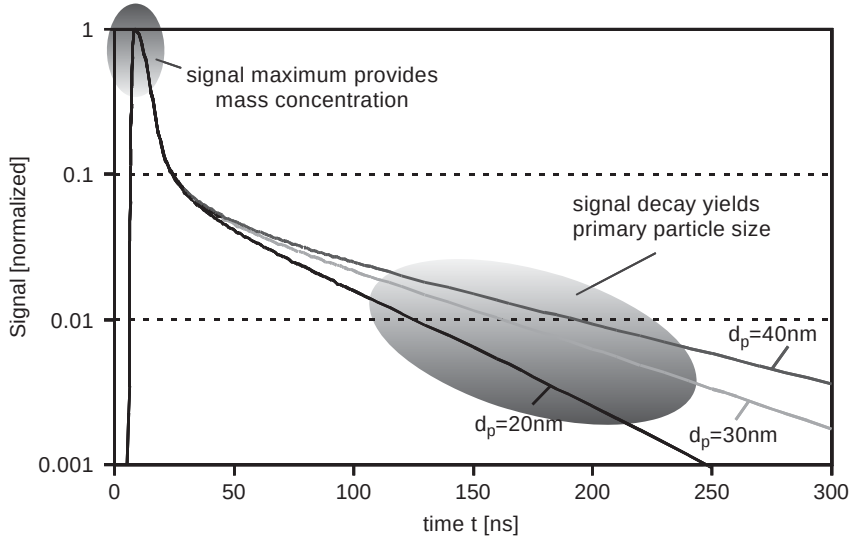

Figure 2 Temporal curve of the LII signal for different primary particle diameters.

detected by using a fast photomultiplier tube (PMT). This procedure, however, allows only the acquisition of pointwise information but this is no drawback in systems with spatially distributed particles owing all the same attributes. If this is not the case, two-dimensionally resolved measurements can be performed providing information over an extended part of the combustion field simultaneously. For this purpose ICCD cameras with short gating times are used. Since there exists a minimum temporal interval between two recordings of a CCD camera, it is only possible to detect the LII signal at certain times after the laser pulse. From the ratio of the signals at different times, the signal decay time can be calculated and processed for each pixel as for the pointwise case. This strategy has been used for the measurements in the flame study section (Chapter III).

For all the other measurements presented in this overview, the temporally resolved LII signals were detected with a fast PMT which guarantees a good signal-to-noise ratio. For times after the laser pulse when heat conduction is the most dominant process for energy release from the particles, the LII signal decay of a monodisperse class of particles is nearly a single exponential. As a first approach, it is reasonable to evaluate the mean primary particle size of this monodisperse particle collective in the following way. From the experimental LII signal curve, a signal decay time τ is determined by an exponential fit in a time interval in which heat conduction dominates particle cooling (Figure 3). This τ is compared to a numerically calculated signal decay time (based on the modeling of the power balance) taking into account the surrounding gas temperature T_0 and assuming a monodisperse particle size distribution with diameter $d_{P,mono}$. Hence, the simultaneous determination of the ambient gas temperature is necessary. Moreover, this means that $d_{P,mono}$ is slightly shifted toward larger particles

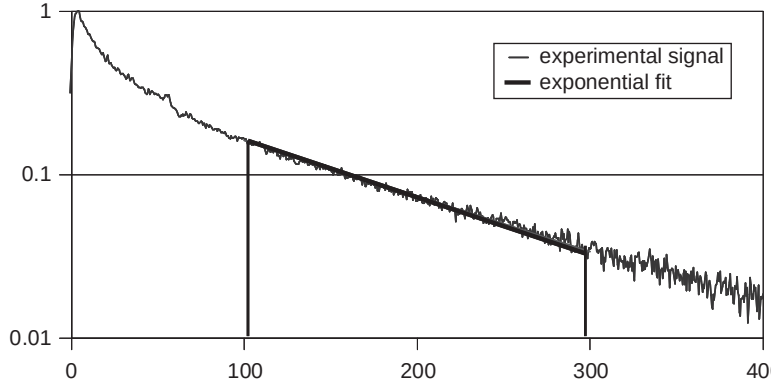

Figure 3 Experimental LII signal with exponential fit.

compared with the medium size $d_{P,med}$ of the real particle size distribution, which is more polydisperse in nature, because the LII signal scales nearly with d_p^3. Thus, TIRE-LII yields this mean primary particle diameter $d_{p,mono}$ without further calibration by comparison of the experimental signal behavior with theoretical predictions since the signal decay can be evaluated independently of the total signal strength.

The accuracy of the technique has first been tested with carbon black particles of the known size as distributed by Degussa AG which also has been used for the investigation of in liquid suspended particles (see Chapter IV.C). In Figure 4, the results are displayed with particles in the size range between 10 and 95 nm (Dankers et al., 2002). Two of the carbon blacks with a primary particle size of 25 nm (Degussa Printex U and Printex 55) had a different aggregate size formed by a different number of primary particles. As the LII measured primary particle size was the same for both aggregates, an influence of the aggregate size on the LII results can be excluded which is true for aggregates with fractal dimensions between 1.5 and 1.9 normally given for combustion-generated soot. This also has been found during carbon black production (see Chapter IV.A.2, Figure 19) and for the investigation of in liquid suspended particles (Chapter IV.C, Figure 39).

A slightly different approach has been introduced by Snelling et al. (2001) and Lehre et al. (2005) which is based on the simultaneous detection of the TIRE-LII signal at two different wavelengths (two-color-LII). By applying Planck's law, the particle ensemble temperature can be calculated from the measured ratio of the TIRE-LII signals at the two wavelengths selected. The major advantage of this technique is that the particle temperatures are experimentally determined independent of the

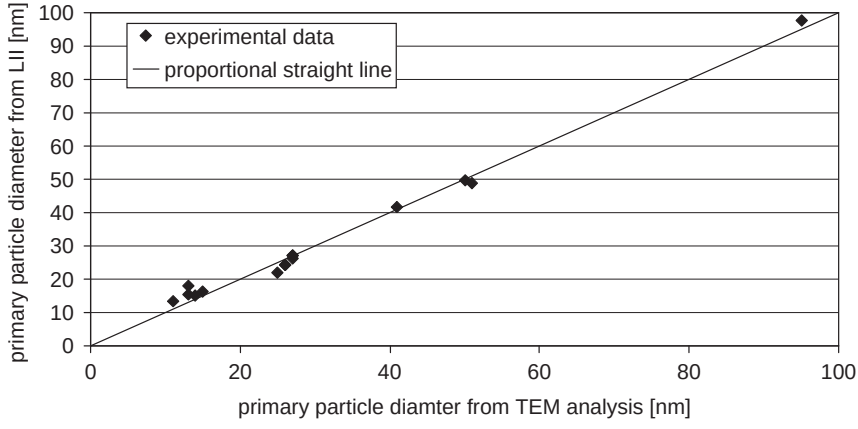

Figure 4 Comparison of LII with TEM.

laser absorption process during the laser pulse which enters most of the models used for simulating the LII signals.

The approach to evaluate the mean primary particle size of a monodisperse particle collective is sufficient if the size distribution is narrow in technical systems, which is typically not always the case. An optional extension of the mean primary particle size determination yields its distribution function. This method relies on the fact that the superposition of several monodisperse signal curves gives, in contrast to monodispersial decay functions, a total signal with a non-exponential shape. In principle, any arbitrary distribution function can be recovered by employing an inverted Laplace algorithm. As this is a very time-consuming issue and is very sensitive to statistical errors and noise on the signal course, a more robust method has to be chosen. One favorable way assumes the presence of any fixed distribution function, which is given by its median diameter and its distribution width. In this case, the shape of the distribution function is assumed to be well characterized by these two parameters. A broadly used and well justified assumption for this distribution is given by a logarithmic normal function

$$P(d_p) = \frac{1}{\sqrt{2\pi} d_p \sigma} \exp\left\{ - \frac{\left[\ln(d_p) - \ln(d_{p,med})\right]^2}{2\sigma^2} \right\} \tag{3}$$

which is typical for combustion processes (Dankers and Leipertz, 2004; Liu et al., 2006a–c). Here, $d_{p,med}$ denotes the count median diameter and $\sigma = \ln(\sigma_g)$ is the width, σ_g being the geometric standard deviation. On the basis of this assumption, higher moments of the particle size distributions can be determined.

Bockhorn et al. (2002) have introduced an approach, by which a calculated signal course is fitted to the whole experimental signal decay under the variation of different distribution parameters such as the width or the mean primary particle diameter. A major drawback of this method is the relative high computing effort for the evaluation which makes the application for online measurements questionable. Roth and Filippov (1996) have introduced an inversion algorithm that also suffers from a complicated and time-consuming calculation procedure and does not lead to unique solutions.

To overcome these deficiencies, a simple online approach has been developed that relies on the fact that the ratio of the contribution to the LII signal of different size classes changes with time after the induced laser pulse. Smaller particles cool down faster, and therefore, a broad size distribution leads to a deceleration of the signal decay as the long-lasting signal of bigger particles become more important at later times. Smaller particles show a faster signal decay and have therefore a constantly decreasing influence on the total signal of the particle collective. This

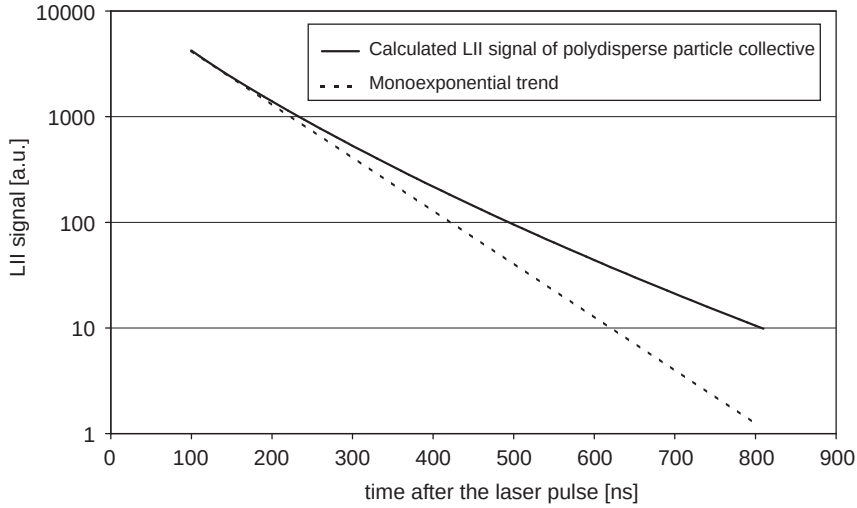

Figure 5 Deviation of the calculated LII signal decay of a polydisperse particle collective (log-normal, $d_{p,med} = 14$ nm, $\sigma = 0.4$) from the monoexponential trend for times after the laser pulse when heat conduction dominates the energy loss (Dankers and Leipertz, 2004).

results in a deviation from an exponential decay, i.e., the signal decay time increases with time (see Figure 5).

For the reconstruction of the size distribution, the theoretical signal course of a particle collective is calculated directly by a weighted summation of LII signals from monodisperse size classes, which are computed from the numerical solution of the power balance. The count median particle diameter $d_{p,med}$, the distribution width σ and the ambient temperature T_0 are input parameter for this calculation. Fitting of this theoretical signal of a size-distributed particle ensemble in two different time intervals after the laser pulse ($(\Delta t)_1$, $(\Delta t)_2$) provides two characteristic signal decay times ($\tau_1 = \tau((\Delta t)_1), \tau_2 = \tau((\Delta t)_2)$).

The calculation of two signal decay times τ_1 and τ_2 can be done under variation of mean particle size, distribution width and ambient temperature yielding the functions $d_{p,med} = f(T_0, \tau_1, \tau_2)$ and $\sigma = f(T_0, \tau_1, \tau_2)$, which are shown exemplarily for an ambient temperature of 1000 K in Figure 6 (Dankers and Leipertz, 2004). It is clearly observable that τ_1 and τ_2 are correlated with σ and $d_{p,med}$ unambiguously. Thus, with the assumption of a certain form of the size distribution, e.g., the log-normal distribution in Equation (3), $d_{p,med}$ and σ can be determined clearly from the experimental curves. To do this the corresponding signal decay times are derived from exponential fits of the experimental data in the selected time intervals.

In Figure 7 this is exemplarily shown for a curve detected in a carbon black reactor with two fits in the intervals 100–300 ns and 400–800 ns after

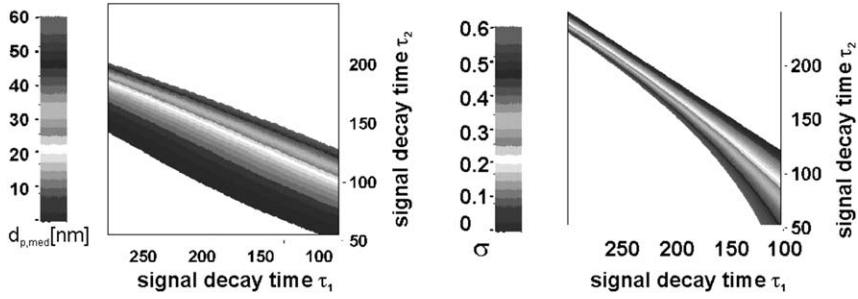

Figure 6 Representation of $d_{p,med} = f(T_U, \tau_1, \tau_2)$ and $\sigma = f(T_U, \tau_1, \tau_2)$ for an ambient temperature of 1000 K (Dankers and Leipertz, 2004).

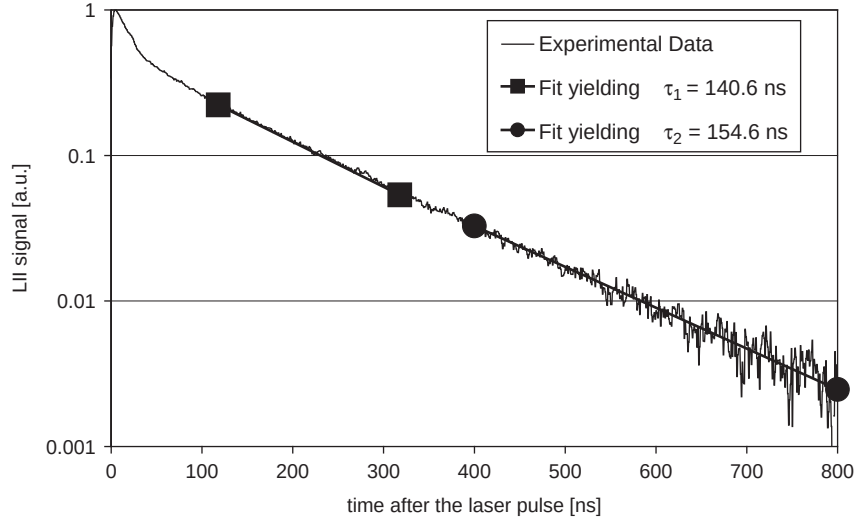

Figure 7 Experimental LII curve with two exponential fits for the reconstruction of primary particle size distribution (Dankers and Leipertz, 2004).

the laser pulse yielding $\tau_1 = 140.6$ ns and $\tau_2 = 154.6$ ns, respectively. The description of the corresponding experimental setup and the performance of the measurements can be found elsewhere (Leipertz and Dankers, 2003). The model signal is not needed in its analytical form; a pre-calculated data base contains only the functions $d_{p,med} = f(\tau_1, \tau_2)$ and $\sigma = f(\tau_1, \tau_2)$ for different ambient temperatures and the fit effort is restricted to two exponential decays.

For the experimental curve shown in Figure 7, under assumption of a long-normal size distribution, the signal decay times yield $d_{p,med} = 32$ nm and $\sigma = 0.11$ which corresponds to a distribution as depicted in Figure 8.

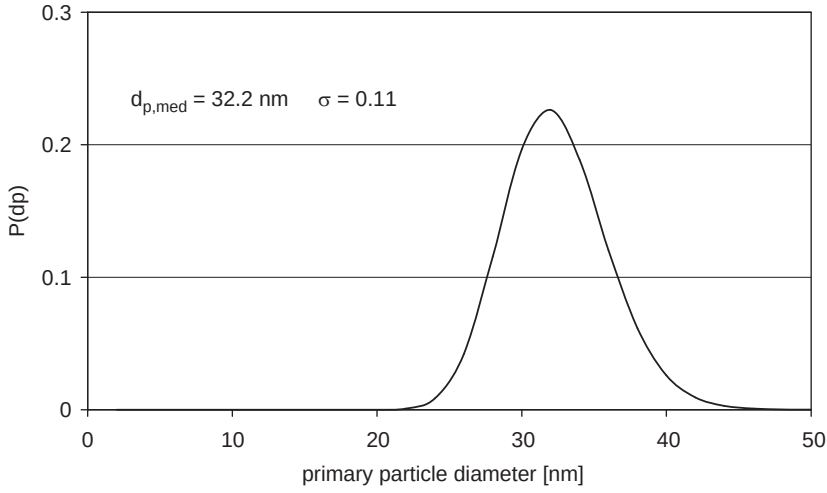

Figure 8 Reconstructed primary particle size distribution by evaluation of the experimental curve shown in Figure 7 (Dankers and Leipertz, 2004).

Assuming a monodisperse particle ensemble, the evaluation of the experimental curve in Figure 7 by only one exponential fit results in the mean monodisperse particle diameter $d_{p,mono} = 34$ nm. For this measurement, it differs only slightly from $d_{p,med}$, since the particle size distribution is rather narrow. Therefore, in this case $d_{p,mono}$ already represents a meaningful and reasonable result regarding primary particle sizing, even though the provision of information about higher moments of the particle size distribution is also valuable.

The choice of suitable evaluation intervals is determined by a compromise between signal strength and significance of the difference in signal decay times. The first interval should begin when heat conduction is the most important energy loss mechanism, i.e., after about 100 ns, and should last for 150–200 ns due to statistical reasons. For the choice of the second interval, the temporal development of the signal decay time must be considered, as it is shown in Figure 9 for the LII signal of two differently size distributed particle ensembles. It is observable that the significance of the differences in the signal decay times for different particle size distributions increases with the time after the laser pulse, so that a later second evaluation interval provides clearer results. However, the signal strength decreases with time, thus signal-to-noise ratio becomes worse. This leads to an increased uncertainty of the determined decay times. So, a suitable interval is to be specified in dependence on the experimental parameters. For high ambient temperatures and/or large particles, the evaluation can be accomplished 600–800 ns after the laser pulse. For other boundary conditions, a second

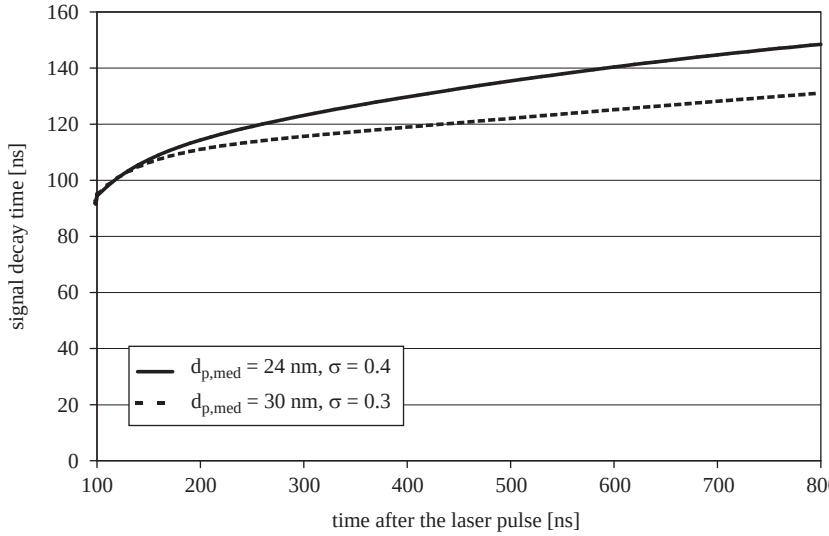

Figure 9 Calculated temporal evolution of the signal decay times for differently distributed particle ensembles (Dankers and Leipertz, 2004).

evaluation interval may cover 400–600 ns or even earlier times. The two evaluation intervals can in principle overlap.

An assessment of the sensitivity of the method is given in Table 1. The effect of a given deviation of the size distribution from starting values on signal decay times in different time intervals after the laser pulse is calculated. A change of $d_{\mathrm{p,\,med}}$ mainly affects the signal decay time τ_1 and results only in a small change of the signal decay time τ_2 in later evaluation intervals. A change of the standard deviation of the size distribution σ, however, has greater influence on τ_2 than on τ_1.

A possible problem is the influence of the aggregate size on the signal decay, when primary particles are packed together to dense structures, which strongly affects the particle cooling (Liu et al., 2006a–c). As shown before (Figure 4), this is typically not the case for aggregates with a fractal dimension between 1.5 and 1.9. Therefore in the measurements presented in the following examples (Chapters III and IV), no shielding effects inside the aggregates are considered.

In principle, however, the effective surface area for heat transfer from the single monomer is decreased by the contact area between the particles. The fractal dimension of the aggregates varies in different systems and depends on the evolution process. For dense aggregates, heat transfer rates are decreased due to the reduced heat exchange area compared to primary particles only connected by point contact in a chain like structure (Liu et al., 2006a–c). This leads to an overestimation of

Table 1 Sensitivity of signal decay times on distribution parameters (Dankers and Leipertz, 2004)

Change of distribution parameter	Start values		Change of signal decay time (%)		
	$d_{p,med}$	σ	τ_1(100–300 ns)	τ_2(400–600 ns)	τ_2(600–800 ns)
$d_{p,med} \pm 5\%$	10	0.2	± 5.2	± 3.9	± 3.6
	20	0.34	± 4.1	± 3.5	± 3.0
	10	0.2	± 3.0	± 5.7	± 6.5
$\sigma \pm 5\%$	20	0.34	± 4.4	± 6.0	± 6.0

expected signal decay rates which results in an overestimation of the primary particle diameters. Basically, a dense aggregate structure can also lead to an alteration of optical properties which can be in principle considered by applying a Rayleigh–Debye–Gans (RDG) approach for the absorption and emission.

3. FLAME INVESTIGATIONS

Fundamental investigations of soot growth and oxidation were performed by many researchers in both diffusion and premixed flames with ethene and methane as fuels (see, e.g., Santoro and Shaddix, 2002; Schulz et al., 2006).

In exemplarily flame measurements conducted at the LTT-Erlangen (Will et al., 1996), flame temperatures were determined by emission spectroscopy or coherent anti-Stokes Raman scattering (CARS) thermometry depending on the maximum soot concentration. Typical temperatures are in the range of 1800 K in the middle of the flames and up to 2100 K in the outer regions where the reactions take place. A typical measurement setup for two-dimensional LII investigations is shown in Figure 10.

In the different flames, the measured concentrations cover a range from 1×10^{-7} to 6×10^{-6} and primary particle sizes range from 2 to 60 nm. Higher soot concentrations and larger particles were measured in the ethene diffusion flame. The resulting maximum number concentration of primary particles, however, is about one magnitude larger in the premixed methane flame. Distributions of the different soot quantities are shown exemplarily for the ethene flame in Figure 11. There is an annular structure in the soot volume concentration observable with maximum values in the outer regions. The concentration decreases in the upper part of the flame where mean primary particle sizes also decrease due to the increasing oxidation of the soot.

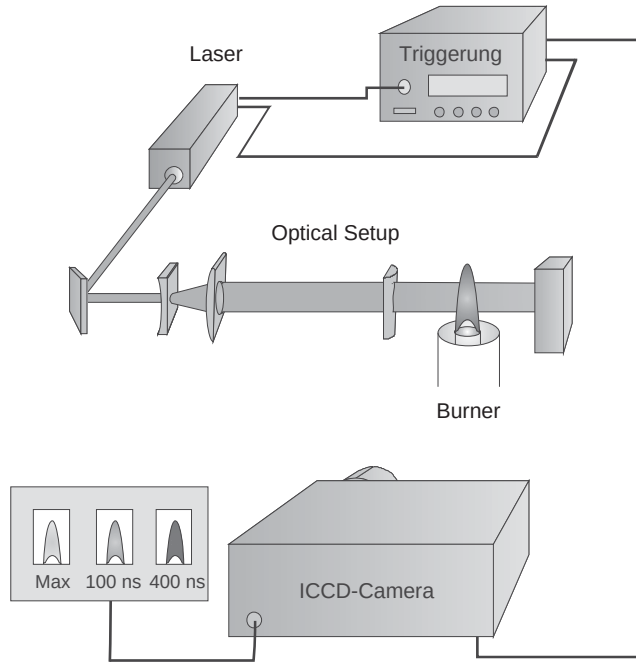

Figure 10 LII measurement setup for two dimensional flame investigations.

4. TECHNICAL APPLICATIONS

In this chapter technical applications are described which are of utmost interest for mechanical and chemical engineers working with particles in the nano size regime. These are the control of production processes of carbon blacks and of non-carbonous and metallic particles, the characterization of soot in automotive applications and the investigation of in liquids suspended particles.

4.1 Control of nanoparticle production processes

Characterization of carbon black primary particle size during the production process was realized at a furnace black production and a research plasma reactor (Dankers et al., 2003; Sommer et al., 2004, 2005).

In Figure 12 a typical LII measurement setup for such applications is shown, whereby here the detection of the enhanced radiation is in perpendicular direction relative to the incident laser beam.

4.1.1 Research plasma reactor

At first the spatially resolved investigation of carbon black primary particle sizes was carried out by realizing a LII setup in backscattering

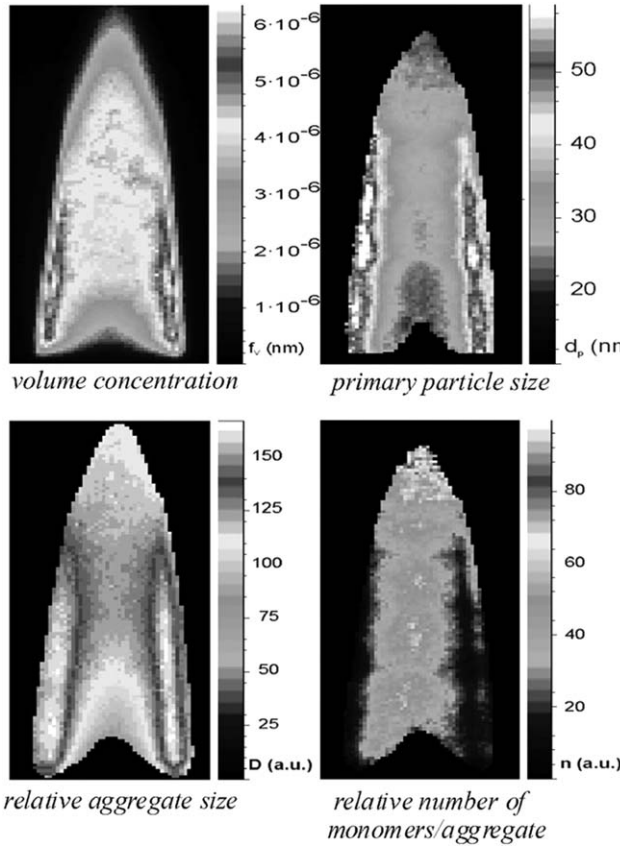

Figure 11 Characteristic properties of soot in a laminar diffusion flame (Will et al., 1996).

geometry within the research plasma reactor (Sommer et al., 2004, 2005). The basic principle of the plasma reactor is the cracking of precursor gas by means of electronically generated plasma and the formation of primary particles out of free molecules.

Unfortunately, at most of technical reactors, only one optical access is available, so LII setups in backscattering geometry have to be realized. Thereby, the carbon black particles are irradiated by a frequency-doubled Nd-YAG laser beam being led into the measurement volume by a mirror and a beam splitter, which are both highly reflective for 532 nm and transmittive for other wavelengths. The LII signal is detected within an appropriately selected spectral range by a fast PMT, fed to an oscilloscope, processed and evaluated by a computer. In the regarded plasma reactor optical access was possible at three different downstream positions (see Figure 13). To obtain an appropriate radial resolution, glass

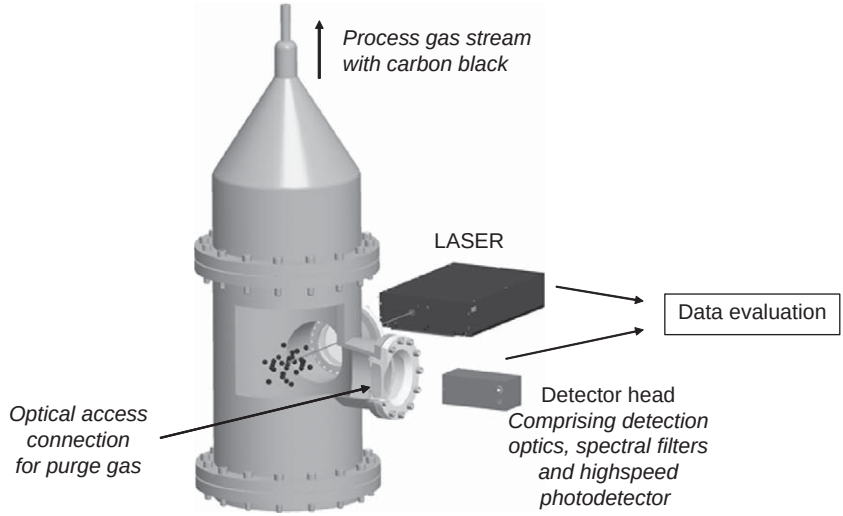

Figure 12 LII measurement setup at a carbon black reactor.

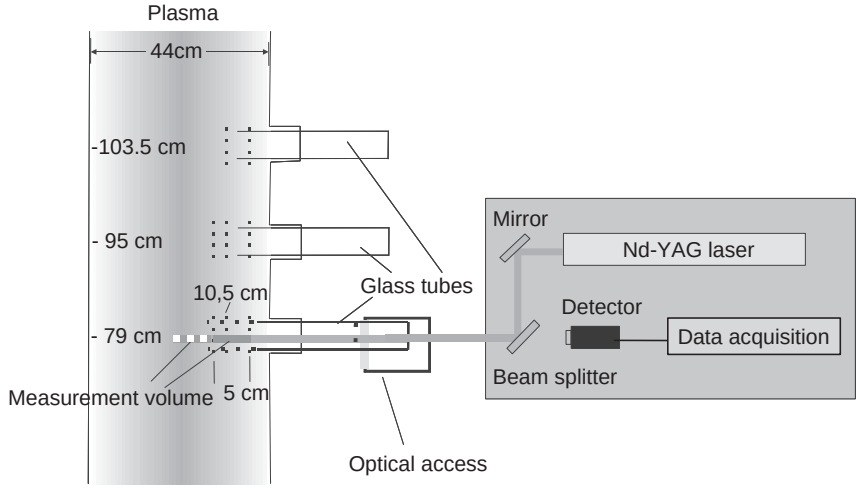

Figure 13 Backscattering configuration at a research plasma reactor (Sommer et al., 2004).

tubes were pushed into the reactor and kept free of carbon particles by means of purge gas. Absorption of the laser beam is so strong that the laser energy is sufficient to heat up the particles only at a short distance after entering the reactor, if the carbon black concentration is high enough. Thus, the outside edge of the LII measurement volume is determined by the end of the glass tubes, as the laser beam cannot

irradiate particles until entering the reactor. However, in the course of the measurements it turned out that the carbon black concentrations were lower than expected, and absorption of the laser beam within a short distance (<1 cm) was not given. The laser irradiance was sufficient to induce incandescence over a long path within the reactor. Thus, the local allocation of the measuring volume became difficult as the signals are integrated over a certain radial distance. Furthermore, additional measurements with a 90°-setup configuration were carried out in order to compare these results with the results of the backscattering geometry. Thereby, the LII signal is detected through a second optical window perpendicular to the laser beam which could only be realized for the lowest local position inside the plasma reactor. The temperature distribution in the reactor was measured with thermocouples which is reasonable for the relatively low carbon black concentrations. The radial temperature gradient is steeper than the axial one which particularly holds in the upper part of the reactor.

For all examined reactor adjustments within the optically accessible range, temperatures do not exceed 1000°C, i.e., the particle formation is expected to be terminated. As the temperature is an important input parameter for evaluating the primary particle size, in case of the backscattering geometry the diameter can only be determined under consideration of the temperature range in the respective measurement downstream position. Nevertheless, these primary particle sizes reveal a good correlation with the results obtained in a perpendicular setup configuration and with calculated particle sizes based on the surface area from chemical analysis. Determinations in different downstream positions provided identical particle sizes for each reactor setting (Figure 14) which is in good agreement with the results of Brunauer-Emmett-Teller (BET) analysis (Table 2) (which is a standard evaluation technique for carbon black size determination) and with the expectation that primary particle formation has already been terminated.

As stated above (see Chapter II.B), LII signals also contain information about the size distribution. To compare the influence of different plasma powers on primary particle diameters, different ways of size evaluation have been accomplished. It could be shown by assuming a monodisperse distribution that the mean primary particle diameter is 31 nm for 30 kW and 33 nm for 70 kW. In contrast, under the assumption of a log-normal distribution and by applying the two-decay time evaluation, the determination yields a different result which can be seen in Figure 15. Size distributions with median sizes of 17 nm and 28 nm and standard deviations of 0.39 and 0.18 for 30 kW and 70 kW were observed, respectively. This indicates that in practical production systems, the evaluation of a mondisperse distribution is not sufficient. Unfortunately, the reconstruction of particle size distributions is relatively sensitive on

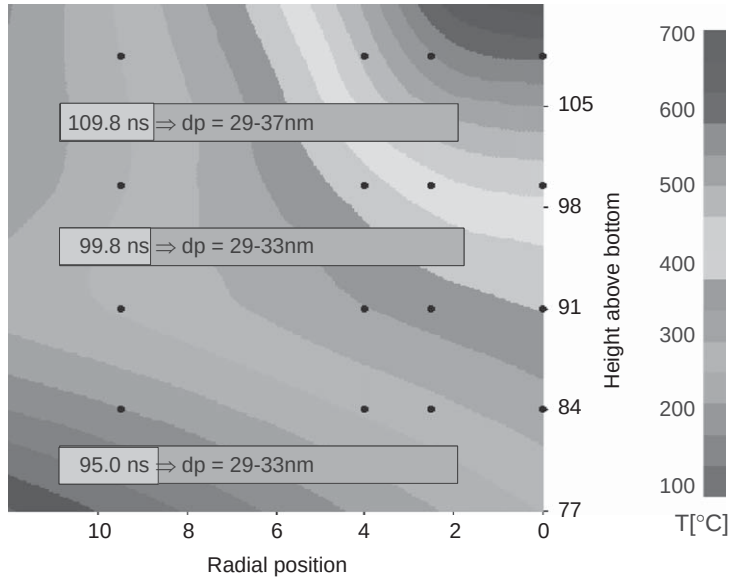

Figure 14 Temperature and calculated size distribution within the plasma reactor (Sommer et al., 2004).

Table 2 Primary particle size d_p derived from LII measurements and BET analysis (Sommer et al., 2004)

d_p (nm) 90°-Setup	d_p (nm) Backscattering geometry	BET (nm)
—	29–35	31
29	29–32	31
33	30–34	33

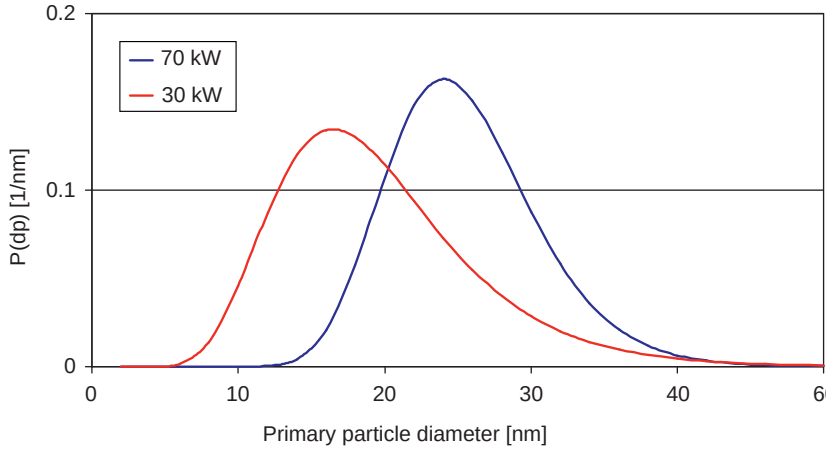

Figure 15 Primary particle size distributions for different plasma power (Sommer et al., 2004) (see Plate 18 in Color Plate Section at the end of this book).

the signal behavior, and therefore, a good signal-to-noise ratio is required.

4.1.2 Furnace black reactor

A similar experimental setup was used to perform online size characterization during the production process within a furnace black reactor (Dankers et al., 2003). During the first series of measurements at a production reactor, it was examined whether phased variations of the operating parameters of the reactor and the resulting changes of the particle size can be observed with the LII technique. It is shown (Figure 16) that the seven different reactor settings can be differentiated clearly by LII, and changes in the primary particle size are detected. The statistical fluctuations during one operation condition are comparatively small.

During the individual phases, carbon black was sampled in order to determine the iodine number. The iodine number results from an adsorption measurement and represents a measure for the specific surface which correlates with the primary particle diameter. Remarkably is that micro porosities of the surface of the particles influence the iodine number. For the comparison of the results from the laboratory analysis and from LII for each phase (duration approximately 20 min), an averaged diameter was determined from the LII signal decay times. Figure 17 shows the outstanding correlation of the results of the two methods for the reactor settings from Figure 16. The iodine number can give only an averaged information over one time period whereas LII

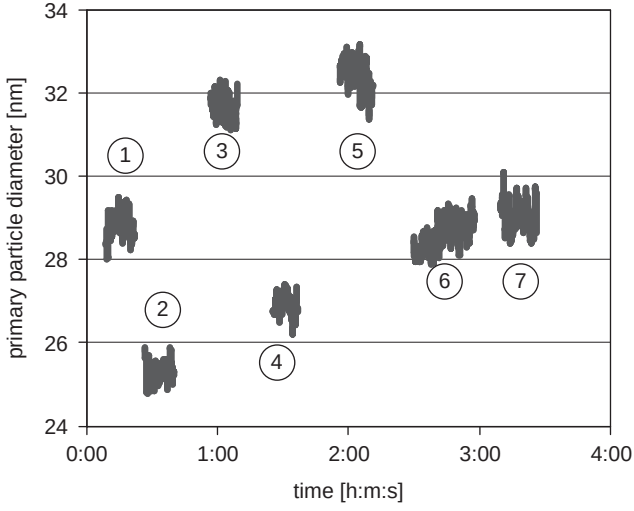

Figure 16 Primary particle size d_p from LII for seven different reactor settings (Dankers et al., 2003).

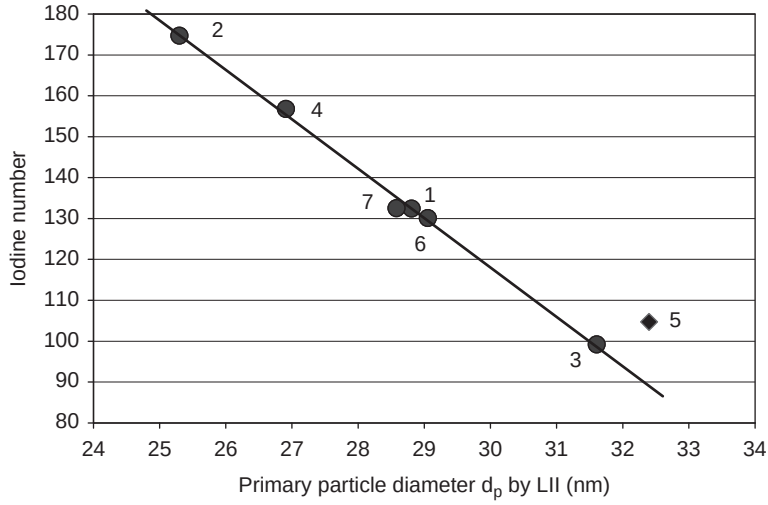

Figure 17 Comparison of the iodine numbers and the averaged d_p from LII with indication of the reactor phase (Dankers et al., 2003).

reacts practically immediately to changes of the measured variable. This highly time-resolved information, however, can be used only with simultaneous and similarly fast temperature measurement. In the measurements described here, the primary particle diameters were computed with the temperature averaged during one period.

Only the results during phase 5 do not fit into the correlation. This is probably caused by the fact that during this phase another position for the water quench to terminate the reaction in the production process had been selected, which affects also the surface porosity apart from the particle diameter. If one assumes that small holes in the surface do not affect the energy loss of the particles after the laser pulse crucially, because the thermal conduction is retarded there, LII determines an enveloping primary particle diameter independently of porosity. The iodine number, however, rises with porosity.

Only then a correlation of the LII results with the iodine number is to be expected if different specific surfaces are caused by variations in the primary particle size and not in porosity. The assumption that LII determines a measure for the enveloping surface without consideration of small porosities has been examined in further measurements at a test reactor of the Degussa AG with finer parameter variations. The aim was to manufacture carbon blacks of same primary particle size, but different surface structure.

Hereby, it was important that the reactor ran stationary. This is contrary to the measurements described before, where very strong parameter variations had been made and therefore small fluctuations of reactor stability had no significant influence. Now a reactor setting was

maintained over several hours, in order to achieve stable operating conditions. Samples were taken for the determination of the iodine number (surface inclusive porosity), the Hexadecyltrimethylammoniumbromid (CTAB) value (represents particle size without consideration of small porosities) and the Dibutylphthalat (DBP) value (measure for the aggregate structure). An exact allocation of the LII results to the laboratory values determined from the samples makes an exact determination of the time interval necessary which the carbon black particles need to travel the way from the LII measurement location directly in the reactor to that place, where the sample is taken, i.e., at the end of the reactor. Since sampling of one probe takes several minutes, the LII signal decay time must be averaged during an appropriate time period. An average period of approximately 20 min that particles spend in the line had been determined already in former times empirically. Therefore, for the comparison of LII with the laboratory analyses, the average value of the LII results 20–15 min before sampling was calculated. The results of the variation of porosity are depicted in Table 3.

The first change leads to a reduction of the iodine number of about 10%, whereby the reduction of the CTAB number is smaller, which points out an increase of the primary particle size with change of porosity. In the next phase obviously larger primary particles (CTAB number decreases) with a more porous surface (iodine number remains constant) are produced. The last variation results in an increase of porosity with nearly constant CTAB number. The LII results correlate clearly with the CTAB number.

In a further series of measurements, the independence of the LII results from the aggregate structure, found in preliminary investigations in a measuring chamber (Chapter II.B), was checked. Differently aggregated particles of similar primary particle size were examined.

The Figures 18 and 19 contain the results of all examined operating points of both series of measurements. The primary particle size from LII does not show systematic dependence on the DBP value which again is a standard evaluation technique in carbon black production (Figure 18).

Table 3 Results of the measurements regarding the variation of porosity (Dankers et al., 2003)

Phase	Iodine number	CTAB value	Primary particle size by LII [nm]
1	206	157	27.0
2	179	155	27.9
3	179	148	29.9
4	190	149	29.5

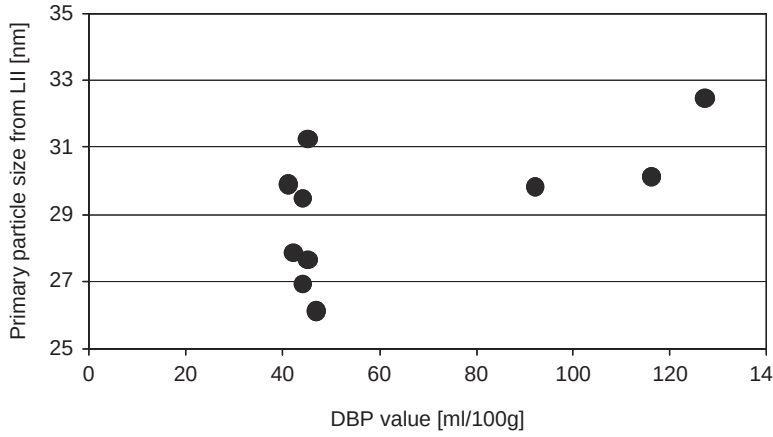

Figure 18 Primary particle size from LII as a function of the DBP value (Dankers et al., 2003).

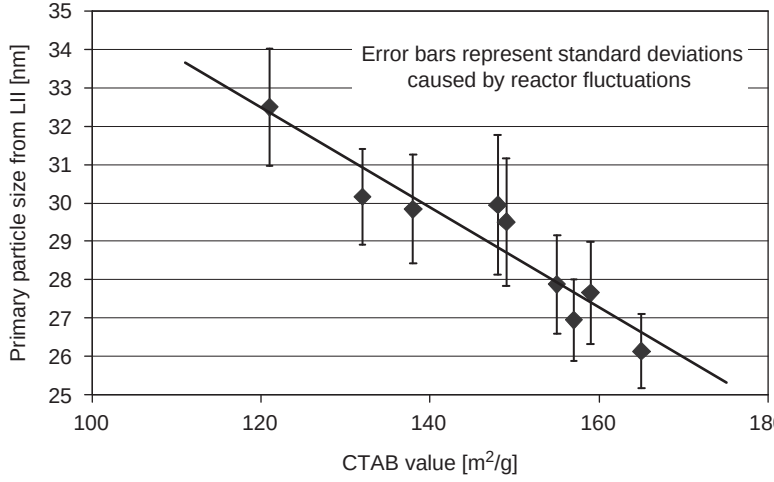

Figure 19 Correlation of primary particle size determined by LII and CTAB value (Dankers et al., 2003).

In Figure 19, however, a clear correlation of the primary particle diameter determined with LII and the CTAB number — the specific surface without consideration of micropores — is observable. The error bars result from the standard deviations of the average values.

It is to be noted that the size of the standard deviation is determined by fluctuations of the particle size, i.e., among other things by reactor fluctuations, and is not a characteristic of the measuring technique as it was already shown in laboratory tests at stationary objects free of doubts.

4.1.3 Metal and metal oxides production reactors

First investigations of metals and metal oxides indicated the principle applicability of LII also for these particles (Filippov et al., 1999; Vander Wal et al., 1999; Kock et al., 2005). Here problems may arise from the particle properties entering the energy balance, e.g., the complex refraction index, which are often unknown. In order to overcome these dependences, a new approach has been introduced by Snelling et al. (2002) and Lehre et al. (2005) using two different wavelengths (two-color-LII) which has already been described in Chapter II.A. Thereby, the temperature signal can be directly obtained from the fraction of both wavelength signals. For particle systems with unknown optical properties, this is an advantageous method for LII particle characterization.

4.1.3.1 Laser vaporization reactor. At LTT-Erlangen, first investigations with other nanomaterials have been carried out in cooperation with the group of Staupendahl at the University of Jena in a laser vaporization reactor (LVR) (Staupendahl, 2003). The basic principle of this reactor is dispersing raw material by a fountain into the CO_2 laser beams, in which particles are vaporized and nanoparticles are formed by the subsequent condensation. As the LII measurement volume was located slightly above the vaporization zone, it was not possible to prevent coarse structures of material to occur inside the measurement volume (Figure 20).

Thereby, LII signals could be detected for ZrO_2 and TiO_2 by varying laser excitation wavelengths from 532 nm to 355 nm. It turned out that UV excitation yields a clearly improved LII signal for TiO_2 (Figure 21).

Thus, a quantitative evaluation of the particle size was impossible at that time, as coarse pieces had been constantly contributing to the detected LII signal. This is confirmed by the fact that the detected signal decay can be explained very well under the assumption of the superposition of two signal contributions, i.e., a fast dropping signal from nanoparticles and a long-lasting signal of coarse structures of the raw material (Figure 22).

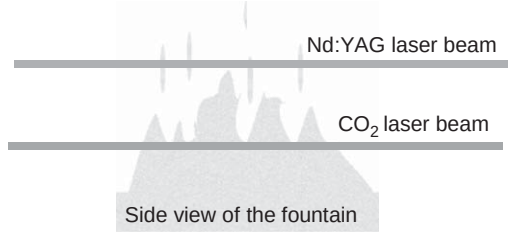

Figure 20 Side view of the dispersing fountain in the LVR (Sommer et al., 2004).

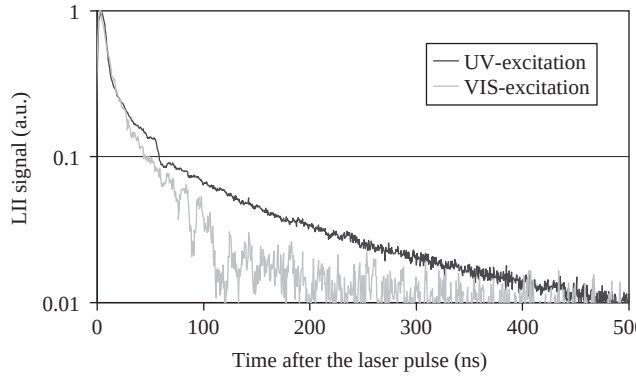

Figure 21 Typical LII courses of TiO_2 with different laser excitation wavelengths (Leipertz and Dankers, 2003).

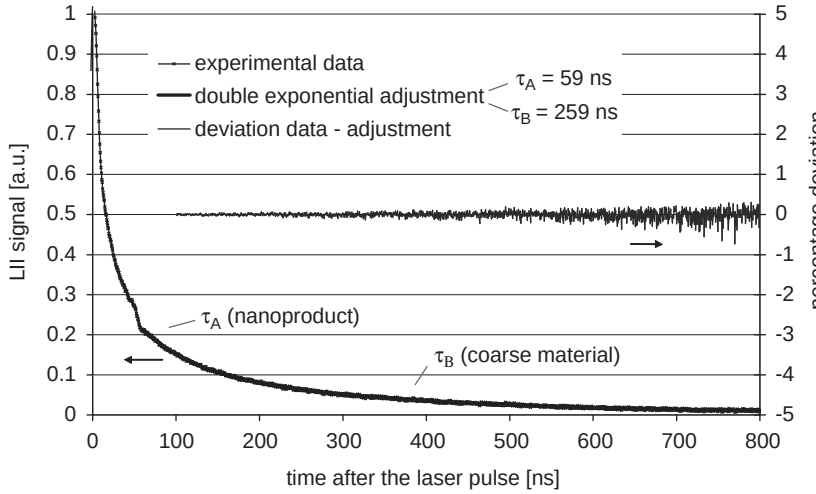

Figure 22 LII signal with double exponential adjustment (Sommer et al., 2005).

The changing mass ratios, however, do not allow a separation of the signals. To prevent these disturbances further investigations were carried out in backscattering geometry at a different LVR without a fountain (Figure 23). LII signals could be detected besides the already mentioned materials also for Fe_2O_3 and MnO_2. For these the influence of CO_2 laser power and pulse length could be examined. The influence of CO_2 laser power on LII signals of Fe_2O_3 is exemplarily shown for various laser powers in Figure 24. It could be shown that the signal maximum which is proportional to the mass concentration increases with rising CO_2 laser power, whereas the signal decay time decreases. Thus, higher concentrations of smaller primary particles were induced by high laser power.

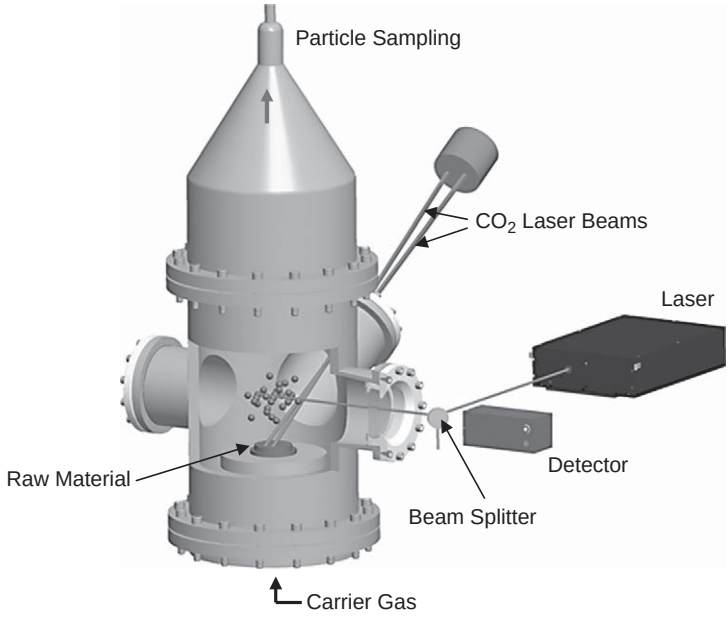

Figure 23 LII setup at the LVR.

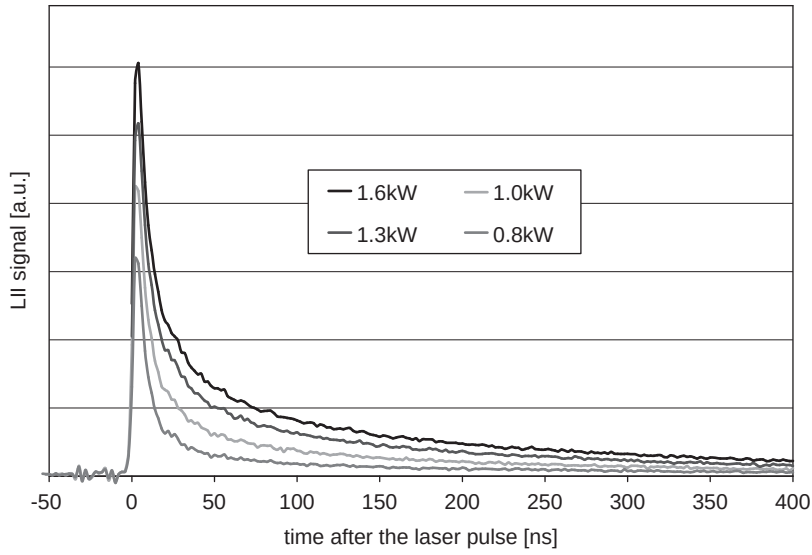

Figure 24 Influence of various CO_2 laser power on LII signals of Fe_2O_3 (Sommer et al., 2005).

Contrary to this only an increase of mass concentration but no alteration of primary particle size with longer pulse length could be observed. A similar behavior has been found for MnO_2. Although not real quantitative, the obtained information provides clear directions for further improvement of the production process.

4.1.3.2 Hot wall reactor. Another interesting and trendsetting investigation has currently been carried out in a hot wall reactor. Here, catalytic active iron particles are produced by thermal-induced metal-organic chemical vapor deposition (MOCVD) acting as formation basis for the growth of carbon nanotubes. In this case, a substrate (Al_2O_3 powder) was calcined over 2 hours at 400°C in a hot wall reactor by means of a fluidized bed under helium atmosphere (flow velocity: 265 ml/min). The actual production of the iron nanoparticles takes place by the decomposition of the deployed precursor from type [(arene)(diene)Fe(0)] at temperature of 150°C on the substrate surface (Michkova et al., 2006). Thereby, the precursor was vaporized at 80°C in advance. To monitor the growth of the iron particles, the LII measurement technique was applied at this reactor. A typical Fe particle deposited on the Al_2O_3 surface is shown in Figure 25.

Investigations were carried out by focusing the laser beam of a frequency doubled Nd:YAG laser in the upper part of the fluidized bed by means of a wavelength selective mirror at 532 nm which is described in more detail elsewhere (Leipertz et al., 2008).

In order to prevent vaporization effects, a low fluence approach was chosen. To consider the growth of the particles, the exponential signal decay time was determined. For this, the measurements were carried out

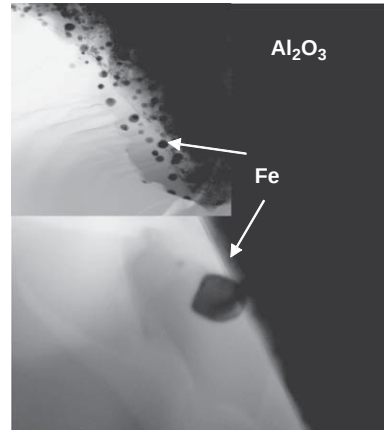

Figure 25 TEM: Fe on substrate (Leipertz et al., 2008).

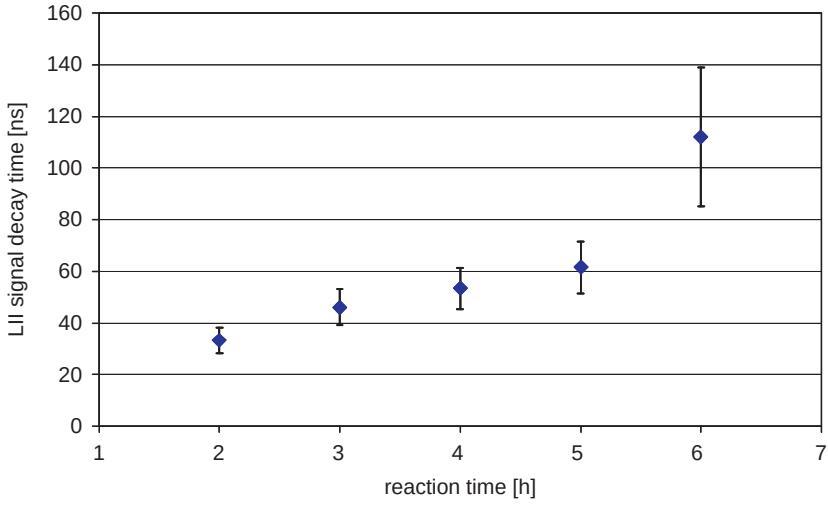

Figure 26 Experimental signal decay time in dependence of the reaction time (Leipertz et al., 2008).

every hour for 2 minutes by opening the heating coil which is coating the glass reactor.

An increase of the signal decay was found in the course of time, which is illustrated in Figure 26, indicating the particle surface growth. It was observable that up to 5 hours a permanent increase of the particles was given. After 6 hours a large rise of the signal decay time was found and a broadening of the experimental standard deviation was measured. This behavior can be explained by slightly removing the iron particles, thus altering the heat conduction, which can be directly seen in the LII signal decay time and was also found by TEM.

For size quantification of these particle systems, the underlying LII model has to be extended taking into consideration the optical metal particle properties (Vander Wal et al., 1999; Kreibig and Vollmer, 1995) on the one hand side and the contact surface area, on the other hand. The optical metal properties, which are in particular determined by the high imaginary part of the complex refraction index, show low absorption coefficients.

One important factor that influences the heat loss the most is the heat exchange area between the iron and substrate particle. For a spherical iron particle with a diameter of 120 nm and a gas temperature of about 423 K the temperature decay was calculated in dependence of the contact area which is denoted as the percentile value of the total iron particle surface, which is illustrated in Figure 27.

Smaller contact exchange surface areas cause a slow down of the temperature release due to the dominating gas phase conditions. Comparing the theoretical calculated signal decays in the time frame

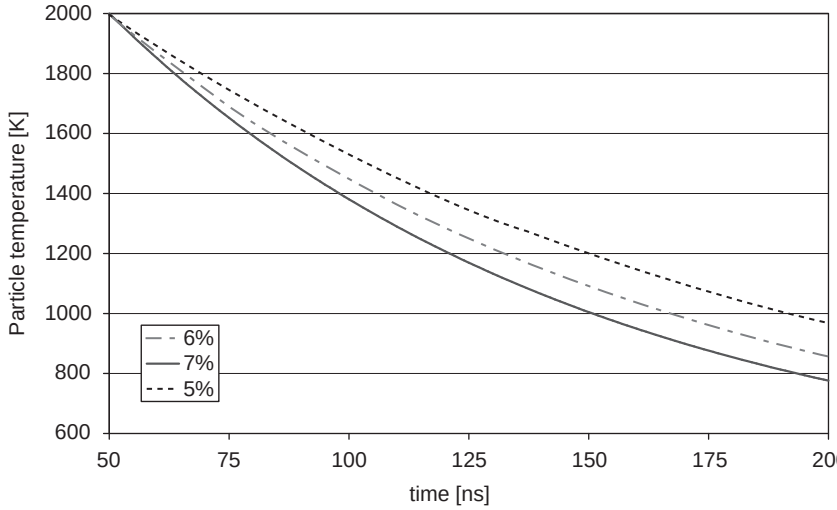

Figure 27 Calculated temperature decay for different percentile contact areas.

between 50 and 150 ns to the experimental ones for a mean primary particle size of 120 nm, which is measured by TEM, is in good agreement. Although the deviation of the LII experimentally determined signal decay times is broad after 6 hours, it is possible to describe these results by the LII model varying the involved parameters. Assuming a mean percentile contact area of 6% also over the whole formation process, the primary particle sizes can be directly determined from Figure 28.

4.2 Automotive soot investigations

Nanoparticles in form of soot play a prominent role in the automotive industry. Soot production, oxidation and emission is an important issue in diesel and gasoline direct-injection engine optimization as this is one of the pollutant components covered in legislation rules to be fulfilled by engine manufactures. TIRE-LII is a very suitable tool to control the soot distribution inside the engine combustion chamber and in the raw exhaust gas (Schraml et al., 1999). In combination with standard NOx measurement in the engine exhaust, TIRE-LII can be used for engine optimization (Schmid and Leipertz, 2006). In engine raw exhaust investigation, LII is only sensitive to elemental carbon (EC). Possible particle components such as ashes, soluble and volatile fractions are not determined, as they are vaporized by the high intense laser pulse.

4.2.1 LII exhaust gas sensor

For raw exhaust measurements in the automobile industry and fine dust investigations in the surrounding atmosphere, the TIRE-LII technique

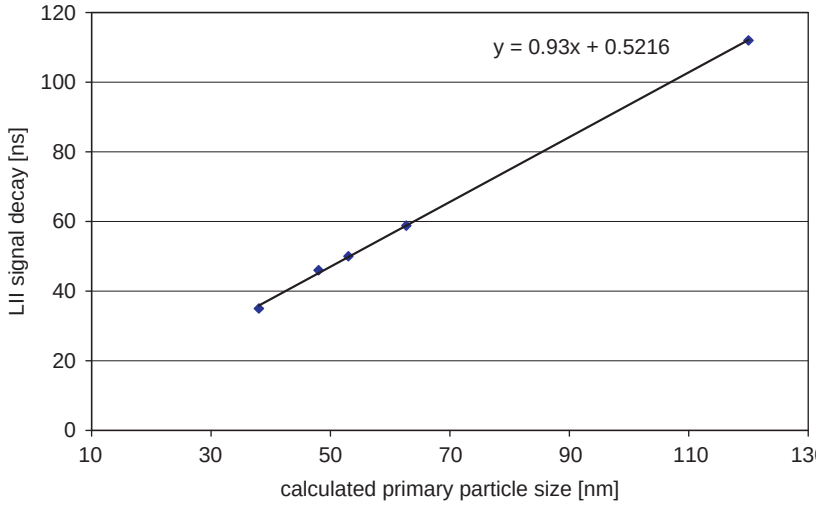

Figure 28 Correlation of experimental signal decay time and calculated primary particle size assuming a percentile contact area of 6%.

has been integrated in a compact sensor (Schraml et al., 2004; Sommer et al., 2005). Selective particle characterization is essential to appraise the performance characteristics of diesel exhaust after treatment systems and of specific engine optimization. For this, real-time investigations are important in order to resolve fast particle property changes.

The system consists of a water cooled ring adapter with purge air supply (Figure 29) and of a control and evaluation unit. The laser beam with an excitation wavelength of 1064 nm is focused in the measurement volume by a light fiber and the enhanced thermal radiation is captured by an appropriate detector head perpendicularly. It can be applied directly in the raw exhaust without dilution up to exhaust gas peak temperatures of 700°C. Its sensitivity (3 $\mu g/m^3$) and variability for real-time (20 Hz) soot characterizing in different applications is shown.

As already published (Schraml et al, 2004), all the other components of the system are integrated into a compact 19'' rack cabinet. The embedded processing computer is responsible for control of the system parameters including laser and detector unit and allows fully automated operation of the system including data acquisition, online evaluation, visualization and storage. The detector gain is adjusted by a control voltage which is automatically controlled by the system processing unit to enable a broad dynamic range which is particularly important for highly transient tests. The signal is recorded by a fast analog-to-digital converter (PCI interface card) which additionally offers the possibility to enlarge the dynamic range. This can be done by adjusting the voltage resolution of the input signal. As the system software dynamically

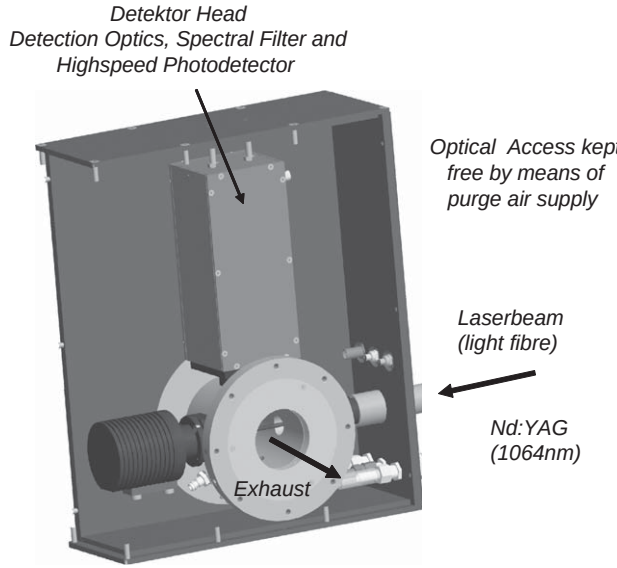

Figure 29 LII soot sensor (raw exhaust ring adapter).

adjusts detector gain and AD converter resolution, the dynamic range of a single setup is currently as high as nearly 10^5. This system is commercially available as Laser-Induced Soot Analyzer (LI^2SA) being produced by the Spin-Off-Company of the Department of Engineering Thermodynamics of the University of Erlangen-Nuremberg. Similar systems are available on the market also from other companies, e.g., Atrium in the USA.

As mentioned before, in engine raw exhaust measurements, LII is only sensitive to EC. This was shown in many previous studies in comparison with conventional standard reference methods such as coulometry, gravimetry or opazimetry (Schraml et al., 2004, and references therein). The only comparable technique that determines only the EC content is coulomteric filter analysis. Therefore, the mass concentration calibration for the sensor is done in comparison with coulometry at a combustion aerosol standard (CAST), which is commercially available from Mattern Engineering in Switzerland and is basically a laminar diffusion flame quenched by a nitrogen flow and equipped with a dilution unit. The soot particles of the CAST system are considered to be very similar to diesel soot in both size and composition if appropriate CAST settings are chosen. By a variation of the dilution air flow different EC mass concentrations can be adjusted in a broad concentration range. In Figure 30 the correlation of the maximal peak LII signal (uncalibrated voltage signal) and the CAST EC concentration setting is depicted. The

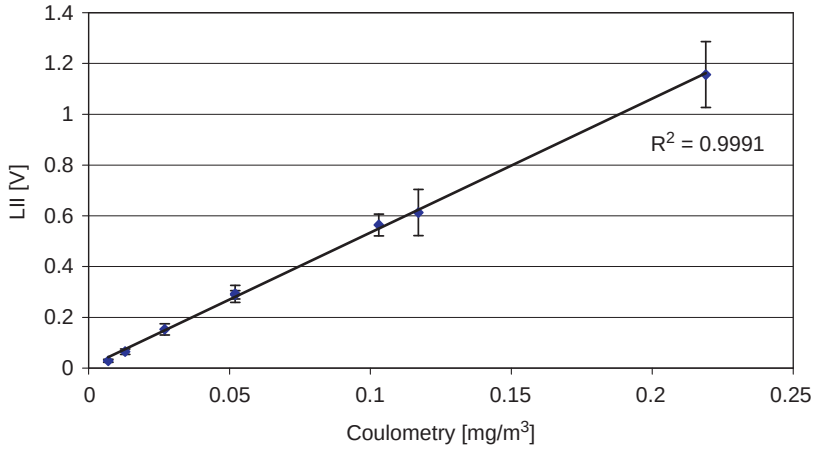

Figure 30 Correlation of the maximal peak LII signal to coulometric filter analysis obtained at a CAST (Schraml et al., 2004).

latter one has been determined by a coulometric analysis of the aerosol flow further taking into account the different dilution ratios.

The error bars of the LII signal are indicating the signal variation (mainly due to fluctuations of the aerosol generator) during the time interval of signal averaging (typically 5 min corresponding to 6000 single measurements). The uncertainty in the coulometric analysis can roughly be estimated with about $\pm 10\%$. Additionally, the figure also gives a first impression about the high sensitivity of the system. From the slope of the graph, a system-specific calibration constant can be deduced.

To verify the results of the determination of the mean primary particle size, the TEM has been applied. To verify the engine exhaust gas measurements in a more adjusted application here additional measurements have been performed again using the CAST aerosol generator operated in different modes. Although just 100–200 single primary particles have been evaluated per test with the TEM method the results are in reasonable agreement with the LII values. It should be pointed out in this context that the statistical error of these measurements is generally much lower than that of TEM as typically up to 10^8 particles (depending on the mass concentration) contribute to the size evaluation. Besides this statistical error, the uncertainties in Table 4 also include temporal fluctuations of the aerosol generator.

4.2.2 Raw exhaust gas measurements

The system has been applied in several configurations on various test benches within different projects, which are here just briefly reported to

Table 4 Comparison of primary particle diameters of TEM and LII obtained with the CAST aerosol generator (Schraml et al., 2004)

Test (diffusion diameter)	d_p TEM (nm)	d_p LI^{2}SA (nm)
CAST 1 (55 nm)	16 ± 2	14 ± 4
CAST 2 (80 nm)	18 ± 3	17 ± 1
CAST 3 (110 nm)	19 ± 3	17 ± 1
CAST 4 (220 nm)	38 ± 2	44 ± 1
CAST 6 (110 nm)	17 ± 3	16 ± 1
CAST 8 (55 nm)	16 ± 3	13 ± 3

illustrate the broad applicability and performance of the TIRE-LII technique in form of the LI^{2}SA sensor.

One possible application of the LI^{2}SA system is the investigation of strategies for internal pollutant reduction. Exemplarily, this can be performed by a variation of the injection timing of heavy duty engine (MAN D08). The used common-rail-system enables an injection which is independent of the engine speed and the free choice of single injection times.

As shown in Figure 31, by adjusting the main injection positioning and the injection pressure, the soot concentrations could be reduced from about 40 mg/m^3 at the base point to 2.5 mg/m^3 and a simultaneous reduction of NO_x emissions. Moreover, the pre-injection at first showed increased particle emissions.

For the engine optimization, some injection parameters have been changed, which is indicated as part of Figure 31. Thereby, the advantage of this sensor technology for research and development applications could be shown. Because of the high sensitivity of the LII sensor also very low concentrations of the emitted soot mass concentration can be accurately measured. The NO_x concentration was measured by means of conventional exhaust measurement devices. A typical method for NO_x reduction is the variation of the injection start, by shifting it to later injection times. It could be shown that the known correlation between NO_x formation and particle emission is valid also for modern engine combustion processes. The retarding of the injection start leads to a significant increase, whereas the NO_x concentration is decreasing (Figure 32).

Another important research field is the investigation of exhaust gas after treatment systems. Besides its high sensitivity, which is important for the characterization of diesel particle filters and fine dust monitoring, also the fast in situ measurement up to 20 Hz makes it possible to optimize filter regeneration strategies or engine combustion even under highly transient conditions. Especially, the investigation of exhaust after treatment system behavior during different test cycles is a very important

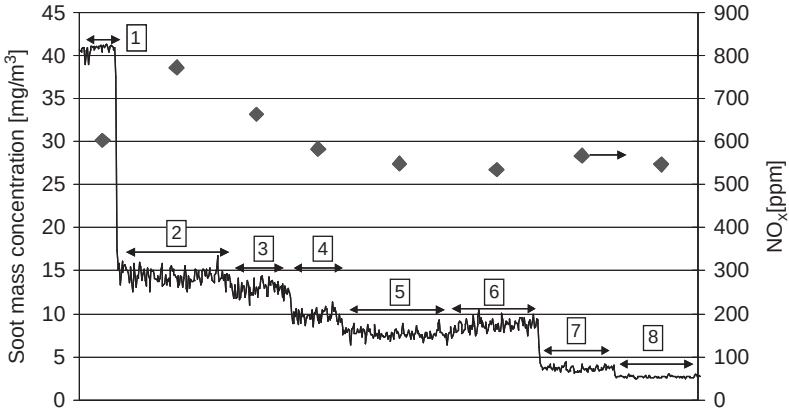

1: Base p_R = 860 bar, SB 3.5° before TDC
2→ 3: increase of injection pressure 860 bar → 1150 bar
3→ 4: positioning of injection 3.5° before TDC → 1.5° after TDC
4→ 5: 1.5° before TDC → 0.5° after TDC
5→ 6: decrease of injection pressure 1150 bar → 1100 bar
6→ 7: without pre-injection
7→ 8: 1.5° after TDC 2.5° after OT

Figure 31 Optimization of an engine operation point (1800 rpm, 605 Nm).

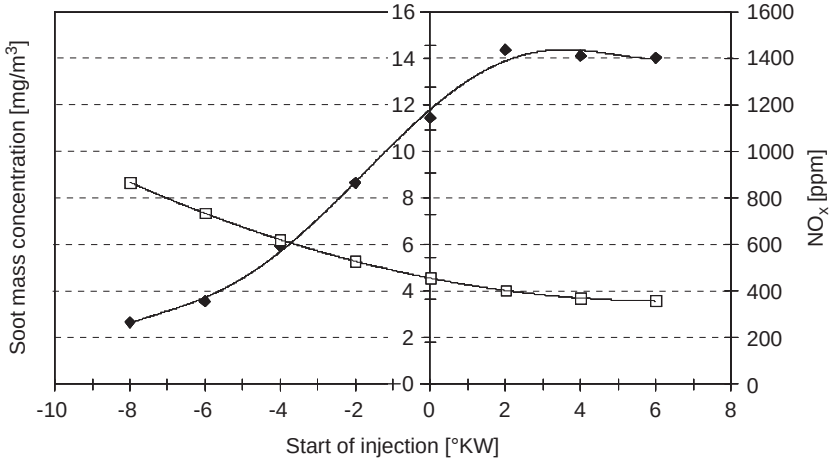

Figure 32 Variation of the injection start (1450 1/min, 313 Nm).

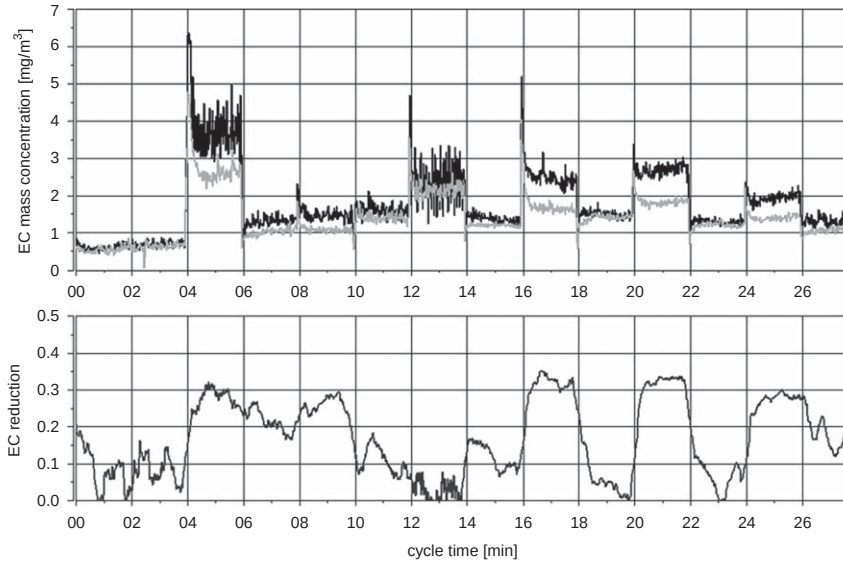

Figure 33 EC mass concentration during ESC test cycle (top) in front of (dark curve) and after (grey curve) a SINOx catalyst and the resulting EC mass reduction (bottom).

task in research and development. In Figure 33 the temporal course of the EC mass concentration is depicted for two different measurement locations during an European Stationary Cycle (ESC) test cycle of a medium duty truck engine equipped with an SINOx© SCR catalyst (SCR stands for selective catalytic reduction) together with the deduced EC mass reduction. The first measurement location was directly in front of the catalyst, whereas the second was immediately afterwards, each utilizing a full-flow sensor head. It could be observed that the EC mass reduction is significantly different for the individual operation points during this 13-stage stationary test cycle. Although the SINOx system has been designed to reduce the nitrogen oxide emission by a selective catalytic reaction after urea injection, an EC mass reduction of about 10–30% was also found. This reduction is strongly dependent on the individual operating conditions, e.g., a significant higher mass reduction occurs under high load conditions. Amazingly, no simultaneous change was observed in specific particle surface or primary particle size (not depicted), respectively. Thus, the dominating reduction process cannot be caused by a particle size reduction in this case, but in particle number. It seems to be most likely that some of the particles passing the SCR catalyst are completely oxidized, whereas other ones pass it entirely unaffected. A possible mechanism is impaction and subsequent oxidization of these particles on the catalyst surface. This example shows that by

selective particle characterization of the mass concentration as well as the primary particle size conclusions can be drawn for the underlying reduction processes in such systems.

Especially the application of particulate filter systems is broadly considered to be the most efficient way for a significant reduction of the soot emission for diesel engines. Consequently, these systems also make high demands on the measurement systems, especially in sensitivity.

In order to simulate decreasing emission levels a truck engine of Euro III emission level (6 cylinder Volvo, displacement 7 liters) has been equipped with a continuously regeneration trap (CRT) filter system and an additional bypass to this filter by the Swiss EMPA institute. By a variation of the flow ratio of filtered/unfiltered exhaust gas, an emission level of about 60% of Euro IV has been adjusted (Mohr and Lehmann, 2003). The temporal courses of EC mass concentration and EC-specific surface area are depicted in Figure 34. In this graph, the mass and surface emissions of the 13 operation points within this test yield a different behavior. Most pronounced is the small specific surface area for idle operation which is caused by relatively large particles and in agreement to the results of previous studies.

Moreover, a CRT-equipped heavy-duty diesel engine was investigated utilizing the partial flow sensor head applied to the secondary dilution tunnel of a full flow CVS system. (Anderson, 2003). In Figure 35 the EC mass concentration during a ETC test cycle is depicted for four consecutive tests. From these measurements, it could be seen that LII is feasible to detect EC mass concentrations with high signal dynamics and

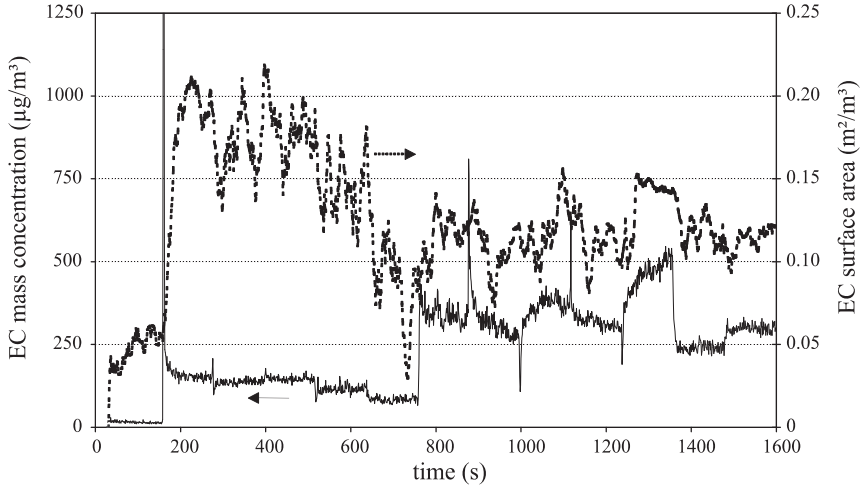

Figure 34 EC mass concentration (dark curve) and EC specific surface area (light curve) during ESC test cycle of a heavy-duty truck engine of Euro IV emission level.

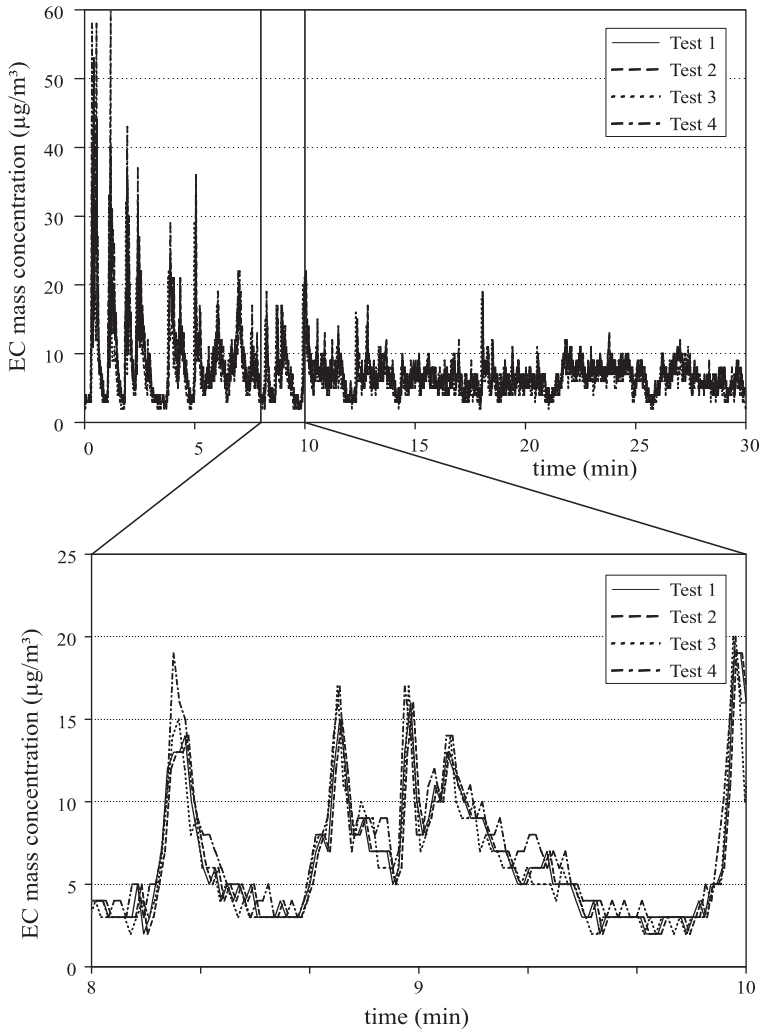

Figure 35 EC mass concentration during four consecutive runs of a ETC (European test cycle) of a CRT equipped heavy-duty truck engine (top: full cycle, bottom: cutout).

high temporal resolutions even at very low, near ambient emission levels. In this application, the very good reproducibility of engine operation conditions for the first time allowed a detailed investigation of the system repeatability under ultra low emission vehicle (ULEV) conditions which has been proven to be excellent (figure, bottom). The discrete steps that are obvious in Figure 34 are just caused by the limitation of the current setting of the measurement resolution (1 µg/m^3, given by

number of digits stored in the recorded data file) rather than by the bit resolution and are therefore no limitation of the dynamic of the AD converter which was automatically adjusted, as discussed above.

Besides measurements on engine test beds, tests on chassis dynamometers are also feasible either with the partial flow or even with a full flow version of the sensor head. Additional to the investigation of diesel vehicles, tests with gasoline-driven vehicles have also been performed (Feest et al., 2003). Here, particular attention has to be paid to modern gasoline direct injection concepts (GDI engines). As a specific example the EC mass concentration of an Audi A4 2.0 liter FSI during a hot federal test procedure (FTP) test cycle is depicted in Figure 36, underlying the applicability of LII also for these concepts.

From Figure 36 it can be observed that the EC emission level from this GDI engine is, speaking in terms of concentration, approximately of the same order than the emission level of a Euro-IV heavy duty truck engine (see e.g., Figure 34) and even one order of magnitude higher if the latter one is equipped with a trap . This is particularly interesting as particulate emission from GDI engines is currently not regulated at all.

4.2.3 Ambient Air Studies

With respect to emission legislation, many European cities transgressed the threshold value of particulate matter exposure. Unfortunately, only the total mass of particles smaller than 10 μm is restricted without distinguishing between different components. Epidemiological studies

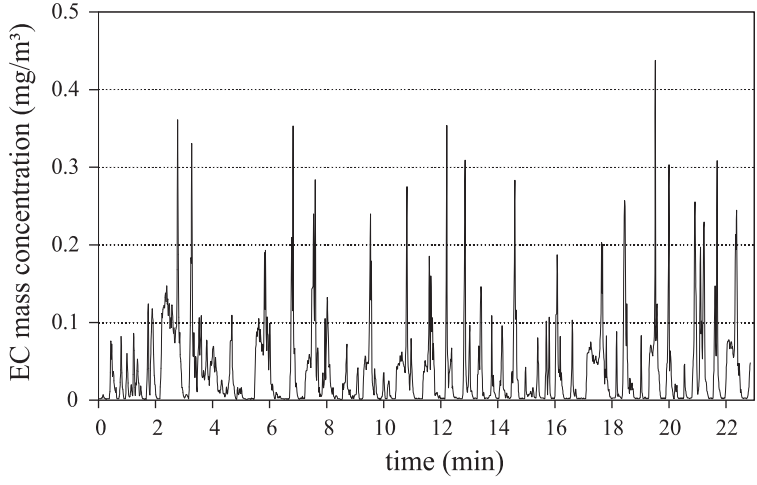

Figure 36 EC mass concentration during a hot FTP test cycle of a Audi A4 FSI equipped with a direct injection gasoline engine (CVS sampling with partial flow sensor head).

indicate that ultra fine particles of definite nature are significantly more dangerous than larger ones. Thus, simultaneous selective determination of mass and specific surface area is necessary to better appraise the exposure composition.

First investigations were carried out next to two different measurement stations, one located at a busy urban road, the other one based at a residential area next to a forest. In comparison with measurements using a tapered element oscillating microbalance (TEOM), which determine the total mass of PM10 per hour, LI^{2}SA characterized the EC fraction averaged in the same time scale. Thereby, at the busy street the mean concentration of EC was always between 7 and 12 μg/m^3. Beyond this, due to the deviation of the non-traffic-related particles, the EC fraction lies always between 20 and 40% of the total mass. By means of time-resolved measurements (5 Hz), short but high peak concentrations were detectable and unambiguous correlation to single vehicles were found when comparing to simultaneously detected video tapes (Figure 37).

Other investigations were conducted at school bus stops to appraise the exposure on pupils. It was found that short (2–6 s) but very high EC mass concentrations of about several hundred μg/m^3 occurred (Figure 38). This underlines the need for comprehensive equipping of buses with particulate traps.

Mobile studies on the road showed the exposure on drivers inside and outside the car (Table 5), whereas the mean EC mass concentration inside the vehicle was approximately doubled. Thereby, specific surface area and primary particle sizes are in the same range as expected. Furthermore, high concentrations at traffic congestions or start ups at

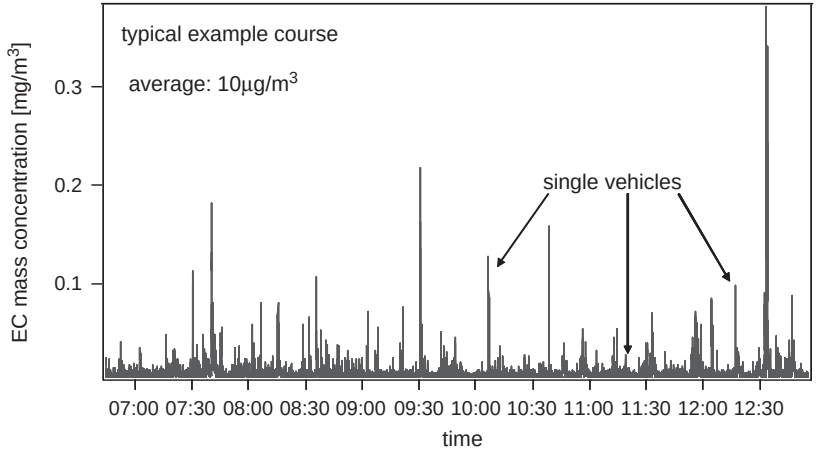

Figure 37 EC concentration at roadside.

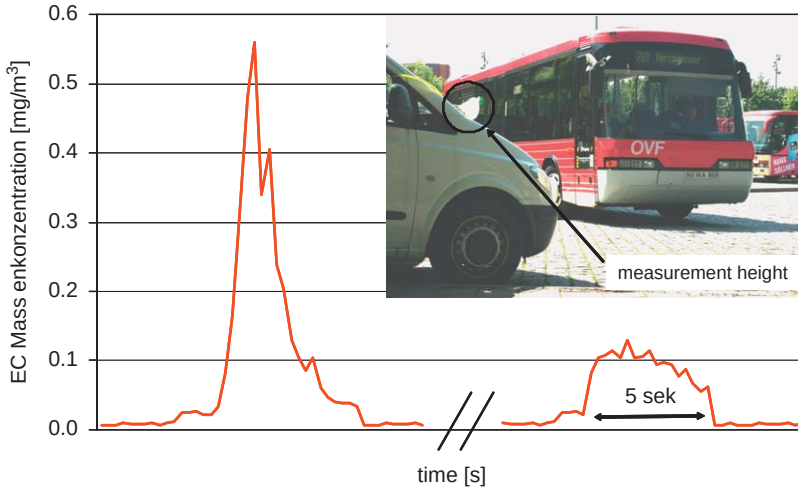

Figure 38 EC concentration at a bus stop.

Table 5 Soot measurements inside and outside the car

	Outside the car	Inside the car
Mean EC mass concentration ($\mu g/m^3$)	8–10	19–28
Maximum EC mass concentration ($\mu g/m^3$)	up to 820	max. 120
Specific surface area (m^2/mg)	0.361–0.067	0.279–0.071
Primary particle size (nm)	11–50	13–47

traffic lights and street crossings can be seen, as well as typical concentration courses inside and after a tunnel.

4.3 Particle suspensions

So far LII has only been applied for aerosol processes without the consideration of particles dispersed in liquids. First, investigations were carried out with re-dispersed carbon blacks. Besides furnace blacks (Printex A, G, 25, 35, and 55), various gas carbon black particles (FW 18, Colour Black S160 and S170, Printex U and U140) were also considered. The particles were suspended in different liquids and dispersed by ultrasonic excitation. The stability of the suspension was recorded by measuring the aggregate size distribution (diffusion diameter) with DLS. Moreover, this was done before and after the LII measurements in order to control the stability of the particle suspension. To achieve LII

excitation, the second harmonic of a Nd:YAG laser at 532 nm having a pulse repetition rate of 20 Hz and a pulse length of 6 ns was used. In order to get a nearly homogenous beam profile, the edges of the laser beam were cut off by passing a 2 mm pinhole. A part of the incident laser beam was reflected by a beam splitter onto the sensor head of a power meter to monitor the initial laser pulse energy. Subsequently, the transmitted laser beam was used for particle heating inside a quartz cell. The excitation energy in the measurement volume was calculated by considering the absorptivities of the quartz cell and of the solvent, the values of which had been predetermined in a test series. The LII signal was collected and imaged on the surface of a fast PMT with a time response of 0.65 ns. In this step elastically scattered laser light was suppressed by using a holographic notch filter. Furthermore, a shortpass filter with a cut-off wavelength of 450 nm and absorptive neutral density filters were inserted for spectrally filtering and signal attenuation, respectively. The PMT signal was digitized by a fast 8-bit analog to digital converter with 250 MHz bandwidth and 1 GS/s sampling rate. Since the temperature of the solvent influences the signal decay, it was determined before and after the LII measurements.

In the course of our investigations, it was possible to detect LII signals for all particle suspensions studied. First, the dependence of the maximal incandescence signal on the laser fluence is documented. The initial increase in laser fluence leads to a rapid rise in the peak LII signal until the sublimation-limited region is reached from which no significant signal change is observable. These results are comparable to those from aerosols and flames as mentioned earlier. Fluence dependency as described here was representative for all carbon blacks tested in this study (Sommer and Leipertz, 2007).

To evaluate the relation of the exponential signal decay time, which is determined 100–250 ns after the laser pulse, and the size of the primary particles, which has been measured by TEM, the laser fluence was set at $0.17\,J/cm^2$. This corresponds to the beginning of the plateau region discussed in more detail in Chapter II.A. A linear correlation between both quantities was found, which is illustrated in Figure 39. No influence of the aggregate size could be found in these investigations. A comparison of Printex U and Printex 55 in particular, which have the same TEM primary particle diameter but different aggregate sizes, confirms this observation, which also has been found before (e.g., Figure 4).

The LII signal decay time was almost the same for both, showing that for the considered carbon black suspensions, the exponential decay time is only a measure of the primary particle size.

In this context, the influence of different solvents on the signal decay behavior was also considered. Despite different thermal conductivities, the signal decay time was not influenced by the solvent in question. This

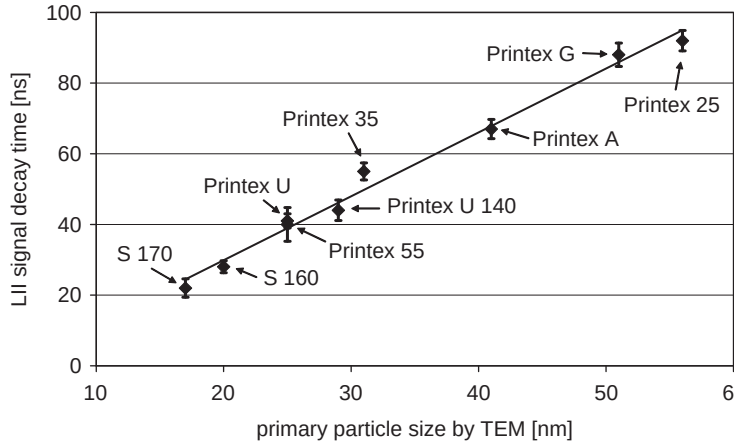

Figure 39 Correlation of LII signal decay time and primary particles size measured by TEM for different carbon blacks dispersed in ethanol (Sommer and Leipertz, 2007).

factor and the signal relation to the laser fluence can possibly be described by vapor layers enclosing the particles, which is described in more detail elsewhere (Sommer and Leipertz, 2007).

Regarding the dependence of the signal decay time on laser energy, a typical course is shown in Figure 40 for Printex G dispersed in ethanol. At first, the signal decay time rises with increasing laser fluence, achieves constant values of about 89 ns in the plateau regime, and subsequently increases. This behavior is characteristic for all carbon blacks and is in contrast to results obtained in a gaseous environment. A possible explanation might be found in solvent vaporization and the formation of a gaseous layer around the particles which directly affects particle cooling. Therefore, the initial increase in the decay time with higher laser fluence could be attributed to a thickening of the vapor layer which leads to an altered heat loss from the particles to the bulk fluid. At higher laser excitations, a gas phase might consist of vaporized solvent and sublimated carbon black. Interestingly, in all studied cases, there is a slight slow down in the signal despite decreasing concentration. This latter behavior is caused in a gaseous environment mainly by particle surface sublimation as mentioned above. However, due to smaller particles, this normally leads to decreasing signal decay times. Increasing decay times, on the contrary, might be referred to particle merging or to a continuous thickening of the vapor layer.

As mentioned before the influence of the liquid on the signal decay behavior was also considered. For this purpose, we worked not only with ethanol but also with isopropanol and methoxy-nonafluorobutane (HFE-7100) because of their different thermal conductivities. Solvent

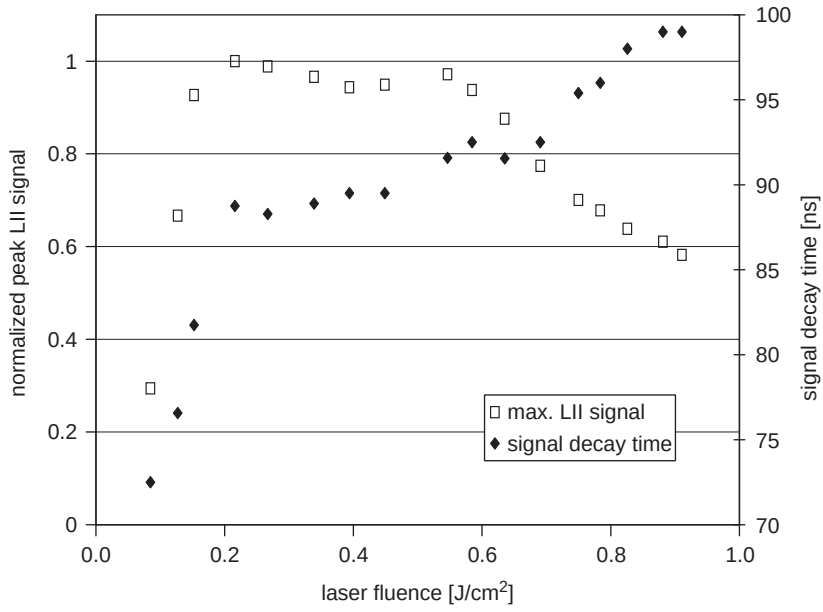

Figure 40 Dependences of the signal decay time and the peak LII signal on laser fluence for Printex G/ethanol suspension.

Table 6 Comparison of LII signal decay times of Printex G for different laser fluences and solvents (Sommer and Leipertz, 2007)

	Decay time (ns)	Ethanol	Isopropanol	HFE-7100
mJ/cm^2	200	89	91	92
	250	90	91	92
	300	90	89	90
	350	92	92	91
	400	91	90	92

temperature was the same before and after the LII measurements. Surprisingly, signal decay time is not affected by the solvent in the plateau region, which can be seen in Table 6. Comparable results are shown for different laser fluences confirming the theory of gaseous layers being formed around the particles.

5. CONCLUSIONS

In this paper the theoretical background and the potentials of TIRE-LII for the determination of the size and mass concentration of nanoscaled

particles has been shown. TIRE-LII has successfully been used for the investigation of soot formation and oxidation in basic combustion research and in two different important technical application fields. The technique has been applied both at different nanoparticle production reactors and directly in engine raw gas exhaust. An online determination of the mean primary particle size of carbon blacks during the particle formation has been carried out and compared to standard chemical analysis indicating very good agreement. Furthermore, primary particle size distributions for different reactor settings were reconstructed by the determination of two signal decay times from the experimental LII signals in comparison with numerically calculated ones. Moreover, the applicability for metal and metal oxide process control was shown in a laser vaporization and a hot wall reactor.

For automotive investigations one of the main benefits of LII, in comparison with conventional particle measurement systems, lies in the exceptional high sensitivity and the possibility of a simultaneous evaluation of EC mass concentration and primary particle size (respectively size of particle surface area). This feature enables a convenient investigation of several interesting effects, which up to now, have not been observed in detail — either because of the lack of possibility or because of the complexity of alternative solutions. Furthermore, the high dynamic range and temporal resolution qualifies LII as an ideal tool for research and engine development as it enables the user to optimize the engine with respect to soot emission even for transient operation conditions. This is particularly important as time-consuming data evaluation is not necessary with this system and so extensive parameter studies can be performed very fast. Therefore, LII is able to comply with all forthcoming developments of new combustion concepts, traps or other exhaust gas after treatment systems. Furthermore, with this measurement technique, it is possible to determine very low soot concentration also in ambient air.

For the first time, TIRE-LII has been successfully applied to the characterization of in liquids suspended nanoparticles. Re-dispersed carbon blacks were investigated in different solvents, whereby a linear correlation between the exponential LII signal decay time and the primary particle size determined by transmission-electron microscopy was found.

TIRE-LII has been found to be a powerful tool for the characterization of nanoscaled particles for basic studies on particle formation and for the investigation of technical nanoparticle applications in mechanical and chemical engineering.

NOMENCLATURE

NOTATION

C_{abs}	absorption efficiency
c_P	specific heat
d_p	particle diameter
E_i	laser energy
ΔH_V	sublimation enthalpy
M	molar mass
M_λ^b,	spectral energy density
T	particle temperature
T_0	temperature of the surrounding

GREEK LETTERS

E	emission coefficient
Λ	heat transfer coefficient
λ	Wavelength
P	mass density
σ	size distribution width
σ_g	geometric standard deviation
τ	signal decay

SUBSCRIPTS AND SUPERSCRIPTS

Med	Median
Mono	Monodisperse

ACKNOWLEDGEMENTS

The authors gratefully acknowledge the financial support for parts of the work by the German National Science Foundation (DFG) and the German Federal Ministry for Education, Science, Research und Technology (BMBF). They additionally thank Degussa AG for support in providing and running the reactors investigated, and furthermore the RWTÜV Institute in Essen and the companies Robert-Bosch GmbH, Argillon GmbH, MAN Nutzfahrzeuge GmbH in Germany within the frame of different projects for enabling the test bench measurements. The LI^{2}SA system has been provided for the measurements by the company ESYTEC Energie und Systemtechnik GmbH in Erlangen, Germany. The Erlangen Graduate School in Advanced Optical Technologies is funded by the DFG in the framework of the Excellence Initiative of the German Federal and State Governments to Promote Science and Research at German Universities.

REFERENCES

Anderson, J. D., "UK particle measurement programme – heavy duty methology development, Final Report Phase 2, Ricardo Consulting Engineers". Shoreham-by-Sea, Great Britain (2003).

Bladh, H., and Bengtsson, P.-E. *Appl. Phys. B* **78**, 241–248 (2004).

Bladh, H., Johnsson, J., and Bengtsson, P.-E. *Appl. Phys. B* **90**, 109–125 (2008).

Bockhorn, H., Geitlinger, H., Jungfleisch, B., Lehre, T., Schon, A., Streibel, T., and Suntz, R. *Phys. Chem.* **4**, 3780–3793 (2002).

Dankers, S., and Leipertz, A. *Appl. Opt.* **43**, 3726–3731 (2004).

Dankers, S., Schraml, S., Will, S., and Leipertz, A. *Chem. Eng. Technol.* **25**, 1160–1164 (2002).

Dankers, S., Leipertz, A., Will, S., Arndt, J., Vogel, K., Schraml, S., and Hemm, A. *Chem. Eng. Technol.* **26**, 966–969 (2003).

Dasch, C. J. *Proc. Comb. Inst.* 231–237 (1984).

Daun, K. J., Stagg, B. J., Liu, F., Smallwood, G. J., and Snelling, D. R. *Appl. Phys. B* **87**, 363–372 (2007).

Feest, E. A., Marshall, I. A., Norris, J. O. W., Reading, A. H., Sandbach, E. L., AEA Technology, Didcot, UK Particle Measurement Programme – Light Duty Methology Development, Final Report Phase 2, Great Britain (2003).

Filippov, A. V., Markus, M. W., and Roth, P. *J. Aerosol. Sci.* **30**, 71–87 (1999).

Hiers, R. *Appl. Phys. B* **92**, 635–641 (2008).

Kock, B. F., Kayan, C., Knipping, J., Orthner, H. R., and Roth, P. *Proc. Comb. Inst.* **30**, 1689–1697 (2005).

Kreibig, U., and Vollmer, M., "Optical Properties of Metal Clusters". Springer Verlag, Heidelberg (1995).

Lehre, T., Jungfleisch, B., Suntz, R., and Bockhorn, H. *Appl. Opt.* **42**, 2021–2030 (2003).

Lehre, T., Suntz, R., and Bockhorn, H. *Proc. Comb. Inst.* **30**, 2585–2593 (2005).

Leipertz, A., and Dankers, S. *Part. Part. Syst. Charact.* **20**, 81–93 (2003).

Leipertz, A., Ossler, F., and Alden, M., *in* "Appl. Comb. Diagns." (K. Kohse-Höinghaus, and J. Jeffries Eds.), pp. 359–382. Taylor & Francis, New York (2002).

Leipertz, A., Sommer, R., Danova, K., Popovska, N., *Proc. CARBON 2008* (2008).

Liu, F., Daun, K. J., Snelling, D. R., and Smallwood, G. J. *Appl. Phys. B* **83**, 355–382 (2006a).

Liu, F., Stagg, B. J., Snelling, D. R., and Smallwood, G. J. *Int. J. Heat Mass Transfer* **49**, 777–788 (2006b).

Liu, F., Yang, M., Hill, F. A., and Snelling, D. R. *Appl. Phys. B* **83**, 383–395 (2006c).

Melton, L. A. *Appl. Opt.* **48**, 4473–4479 (1984).

Mewes, B., and Seitzman, J. M. *Appl. Opt.* **36**, 709–717 (1997).

Michelsen, H. A. *J. Chem. Phys.* **118**, 7012–7045 (2003).

Michelsen, H. A., Liu, F., Kock, B. F., Bladh, H., Boiarciuc, A., Charwath, M., Dreier, T., Hadef, R., Hofmann, M., Reimann, J., Will, S., Bengtsson, P. E., Bockhorn, H., Foucher, F., Geigle, K. P., Mounaim-Rousselle, C., Schulz, C., Stirn, R., Tribalet, B., and Suntz, R. *Appl. Phys. B* **87**, 503–521 (2007).

Michelsen, H. A., Linne, M. A., Kock, B. F., Hofmann, M., Tribalet, B., and Schulz, C. *Appl. Phys. B* **93**, 654–656 (2008).

Michkova, K., Schneider, A., Gerhard, H., Popovska, N., Jipa, I., Hofmann, M., and Zeneck, U. *Apll. Cataly.* **315**, 83–90 (2006).

Mohr, M., Lehmann, U., Particle Measurement Programme (GRPE-PMP) – Comparison Study of Particle Measurement Instruments for Future Type Approval Applications, EMPA Report, Dübendorf, Switzerland, (2003).

Reimann, J., Kuhlmann, S.-A., and Will, S. *Comb. Flame* **153**, 650–654 (2008).

Roth, P., and Filippov, A. V. *J. Aerosol. Sci.* **27**, 95–104 (1996).

Santoro, R. J., and Shaddix, C. R., *in* "Appl. Comb. Diagns." (K. Kohse-Höinghaus, and J. Jeffries Eds.), pp. 252–286. Taylor & Francis, New York (2002).
Schmid, M., and Leipertz, A. *Int. J. Engine Design* **41**, 188–205 (2006).
Schraml, S., Will, S., Leipertz, A., *SAE Technical Paper Series*, 1999-01-0146 (1999).
Schraml, S., Dankers, S., Bader, K., Will, S., and Leipertz, A. *Comb. Flame* **120**, 439–450 (2000).
Schraml, S., Kremer, H., Sommer, R., and Leipertz, A., Proceedings of the 8th International Symposium on Diagnostics and Modeling of Combustion, *in* "Int. Comb. Eng. (COMODIA)" Yokohama, Japan (2004).
Schulz, C., Kock, B. F., Hofmann, M., Michelsen, H., Will, S., Bougie, B., Suntz, R., and Smallwood, G. J. *Appl. Phys. B* **83**, 333–354 (2006).
Shaddix, C. R., and Smyth, K. C. *Comb. Flame* **107**, 418–452 (1996).
Snelling, D. R., Liu, F., Smallwood, G. J., and Gülder, Ö. L., "Proceedings of the 34th National Heat Transfer Conference". Pittsburgh, PA, USA, NHTC2000-12132 (2000).
Snelling, D. R., Smallwood, G. J., Gülder, O. L., Liu, F., and Bachalo, W. D., "Second Joint Meeting U.S. Sections Combustion Institute". Oakland, CA, USA (2001).
Snelling, D. R., Thomson, K. A., Smallwood, G. J., Gülder, O. L., Weckman, E. J., and Fraser, R. A. *AIAA Journal* **40**, 1789–1795 (2002).
Sommer, R., and Leipertz, A. *Opt. Lett.* **32**, 1947–1949 (2007).
Sommer, R., Dankers, S., Will, S., and Leipertz, A., *in* "Handling of Highly Dispersed Powders" (E. Müller, and C. Oestreich Eds.), pp. 32–39. Shaker, Aachen (2004).
Sommer, R., Dankers, S., and Leipertz, A. *Chemie Ingenieur Technik* **77**, 214–223 (2005).
Sommer, R., Kaste, A., and Leipertz, A., "Proceedings of the 9th International ETH Conference on Combustion Generated Nanoparticles". Zürich, Switzerland (2005).
Staupendahl, G., Kurland, H.-D., and Garbow, J., IEEE LEOS Newsletter 17 (2003).
Tait, N. P., and Greenhalgh, D. A. *Phys. Chem.* **97**, 1619–1625 (1993).
Vander Wal, R. L., and Choi, M. Y. *Comb. Flame* **102**, 200–204 (1995).
Vander Wal, R. L., and Choi, M. Y. *Carbon* **37**, 231–238 (1999).
Vander Wal, R. L., and Weiland, K. J. *Appl. Phys. B* **59**, 445–452 (1994).
Vander Wal, R. L., Ticich, T. M., and Stephenson, A. B. *Appl. Phys. B* **67**, 115 (1998).
Vander Wal, R. L., Ticich, T. M., and West, J. R. *Appl. Opt.* **38**, 5867–5879 (1999).
Will, S., Schraml, S., and Leipertz, A. *Opt. Lett.* **20**, 2342–2344 (1995).
Will, S., Schraml, S., and Leipertz, A. *Proc. of the Comb. Inst.* **26**, 2277–2284 (1996).
Will, S., Schraml, S., Bader, K., and Leipertz, A. *Appl. Opt.* **37**, 5647–5657 (1998).